geosciences

Review

The Geochemical and Isotopic Record of Wilson Cycles in Northwestern South America: From the Iapetus to the Caribbean

Richard Spikings [1,*] and Roelant Van der Lelij [2]

[1] Department of Earth Sciences, University of Geneva, 1205 Geneva, Switzerland
[2] Geological Survey of Norway, 7040 Trondheim, Norway; Roelant.vanderlelij@ngu.no
* Correspondence: richard.spikings@unige.ch

Abstract: Isotopic and geochemical data delineate passive margin, rift and active margin cycles in northwestern South America since ~623 Ma, spanning from the Iapetus Wilson Cycle. Ultramafic and mafic rocks record rifting associated with the formation of the Iapetus Ocean during 623–531 Ma, while the initiation of subduction of the Iapetus and Rheic oceans is recorded by continental arc plutons that formed during 499–414 Ma, with alternating compressive and extensional stages. Muscovite $^{40}Ar/^{39}Ar$ dates suggest there may have been a phase of Carboniferous metamorphism, although this remains tentative. A Passive margin was modified by active margin magmatism that started at ~294 Ma and culminated with collisional tectonics that signaled the final stages of the amalgamation of western Pangaea. Early Pangaea fragmentation included back-arc rifting during 245–216 Ma, leading to a Pacific active margin that spanned from 213–115 Ma. Trench retreat accelerated during 144–115 Ma, forming a highly attenuated continental margin prior to the collision of the Caribbean Large Igneous Province at ~75 Ma.

Keywords: Northern Andes; isotopic tracing; geochronology; geochemistry; thermochronology

check for updates

Citation: Spikings, R.; Van der Lelij, R. The Geochemical and Isotopic Record of Wilson Cycles in Northwestern South America: From the Iapetus to the Caribbean. *Geosciences* **2022**, *12*, 5. https://doi.org/10.3390/geosciences12010005

Academic Editors: Olivier Lacombe and Jesus Martinez-Frias

Received: 16 November 2021
Accepted: 13 December 2021
Published: 22 December 2021

1. Introduction

Northwestern South America is a relict fragment of Gondwana and its northern and western margins preserve a punctuated record spanning from the opening of the Iapetus Ocean to its interaction with the thickened Caribbean Plate. Therefore, an improved knowledge of the precise timing and nature of geological events that formed this region is key when reconstructing the configuration of the western regions of Gondwana and Pangea. The objective of this work is to summarise geochemical and isotopic data obtained from igneous and meta-igneous rocks in northwestern South America (Ecuador, Colombia and Venezuela) that are frequently foliated and metamorphosed, with the aim of showing the utility of these data to tightly constrain tectonic reconstructions from the opening of the Iapetus Ocean, closure of the Rheic Ocean, and the evolution of the Pacific margin until the early collision of the Caribbean Large Igneous Province. The studied rock units span between the late Neoproterozoic and the Early Cretaceous (~623–112 Ma).

Data have been compiled from the Cordillera Real and Amotape Complex of Ecuador, the Cordillera Central, Santander Massif and Sierra Nevada de Santa Marta of Colombia, and the Mérida Andes of Venezuela, as well as some geographically scattered locations. The geochemical data are mainly whole-rock major oxide and trace element compositions, which are used to identify petrogenetic processes and thus propose plausible tectonic environments. The isotopic data are used to provide robust geochronological constraints, identify magma source regions and improve tectonic models with the integration of thermochronological information. Geochronological data are mainly restricted to zircon U-Pb concordia ages, although some $^{40}Ar/^{39}Ar$ plateau dates are considered for mafic rocks that did not yield zircon. Radiogenic isotopic tracing uses Nd, Pb (whole rock) and Hf (zircon) compositions, and is complemented with stable oxygen (quartz) isotopic compositions for specific time periods. Thermochronological constraints are provided by apatite U-Pb and $^{40}Ar/^{39}Ar$ muscovite dates, and lower-T thermochronometers including fission track and (U-Th)/He data. These data are compiled into a series of summary figures and identify periods of continental rift-related magmatism associated with the Central Iapetus Magmatic Province and the disassembly of Panotia in the period ~623–531 Ma, Triassic back-arc rift-to-drift magmatism in the period ~245–216 Ma, heralding the early disassembly of Pangaea, and failed rifting during hyperextension of the Pacific margin in the Early Cretaceous starting in ~145 Ma. The older Palaeozoic arc sequences are geographically dismembered and most exposures occur in inboard regions of northwestern South America (~499–414 Ma and 296–250 Ma; Mérida Andes and the Santander Massif, and minor occurrences in the Cordillera Central) during the subduction of Iapetan and Rheic oceanic lithosphere, and in crustal blocks that are dispersed throughout the cordilleras Real (Ecuador) and Central (Colombia), and isolated blocks in Venezuela. More coherent arc sequences form linear belts along the Mérida Andes, Santander Massif and cordilleras Real and Central in the period during 213–112 Ma.

All of these units either have Gondwanan isotopic signatures or host xenocrystic zircons with a Gondwanan U-Pb date spectrum, and thus are considered to have originated within Gondwana after the disassembly of Rodinia via reworking of the Amazonian Craton and the addition of new crust. With the exception of small porphyry-type intrusions, a significant magmatic hiatus throughout northwestern South America in the period 414–294 Ma is accounted for by the transfer of the rifted conjugate Triassic margin from Gondwana to Laurentia during the Triassic.

2. Geological Framework and Previous Work

Basement rocks within Ecuador, Colombia and Venezuela can be divided into allochthonous units that originally formed part of the oceanic Caribbean Plate and thus have juvenile isotopic signatures and are usually ~100 Ma old and younger, or older sequences that are located inboard, are more differentiated and span from the Early Cretaceous to the Precambrian. The suture between these broad regions is dismembered although it is moderately well expressed in gravity maps (Feininger and Seguin, 1983) and is occasionally exposed in the field. The dismembered suture is referred to as the Ingapirca-Peltetec (Ecuador)–Cauca-Almaguer (Colombia) fault system (Figure 1). This review will focus on the crystalline rocks that formed the buttressing margin at ~100 Ma, which are located east of the suture. These include rocks exposed in the Cordillera Real and Amotape Complex of (Ecuador), Cordillera Central, Santander Massif and the Sierra Nevada de Santa Marta (Colombia), the Mérida Andes (Venezuela) and other geographically scattered regions. We only focus on crystalline rocks that formed during the opening of the Iapetus Ocean, and until the early interaction of South America with the Caribbean Plate.

The oldest rocks are fault-bounded slivers of gabbroic to ultramafic rocks of the Huarguallá Gabbro unit within the Peltetec Fault Zone, located along the western flank of the Cordillera Real (Ecuador; Figure 1). These units yield imprecise $^{40}Ar/^{39}Ar$ dates (plagioclase) spanning between 623–531 Ma (including 2 s uncertainties; [1]), and the rocks are considered to have formed part of the Central Iapetus Magmatic Province during the rift stage of the Iapetus Wilson Cycle [1].

Variably deformed and variably metamorphosed latest Cambrian–early Devonian (499–414 Ma) intrusions form large parts of the Mérida Andes [2,3] and Santander Massif ([2,4–6]). Smaller exposures occur in tectonic slivers along the eastern flank of the Cordillera Central (La Aguadita Amphibolites, La Miel Orthogneiss; [7–9]; Figure 1), the Quetame and Floresta massifs [10], the Sierra Nevada de Santa Marta [11], the El Baul Massif [12] and the Llanos Basin [13]. These Palaeozoic igneous units are not exposed in Ecuador, although they reappear in the northern Eastern Cordillera of Peru [14]. Peak upper amphibolite metamorphism in the Merida Andes and Santander Massif occurred at ~467 Ma, and intrusions that are older than ~467 Ma are strongly foliated [2,3]. The La Miel orthogneiss reached peak amphibolite facies [15] and is associated with garnet-bearing amphibolites that formed within a subduction zone environment [16], although the timing of metamorphism is unclear.

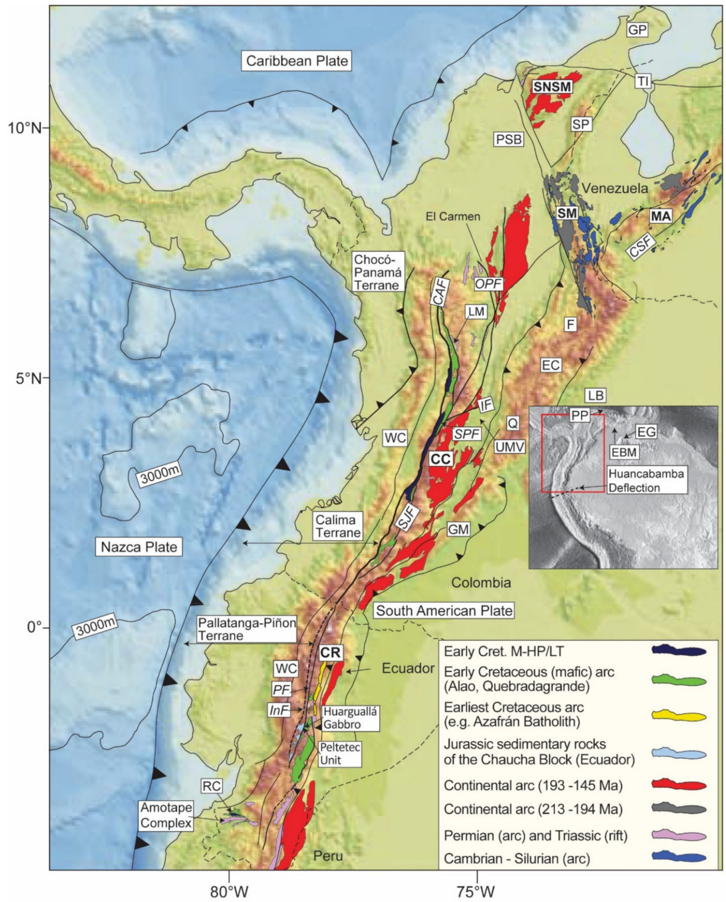

Figure 1. Digital elevation model for northwestern South America showing the cordilleras, terranes, main faults and the exposure of Cambrian–Cretaceous magmatic rocks in Venezuela, Colombia and Ecuador and Colombia. Faults: CAF: Cauca-Almaguer Fault, CSF: Caparo-Soledad Fault, IF: Ibagué Fault, InF: Ingapirca Fault, OPF: Otu-Pericos Fault, PF: Peltetec Fault, SJF: San-Jeronimo Fault. Other abbreviations: CC: Cordillera Central, CR: Cordillera Real, EBM: El Baúl Massif, F: Floresta Massif, GP: Guajira Peninsula, LB: Llanos Basin, LM: La Miel Gneiss, MA: Mérida Andes, OB: Oriente Basin, PP: Paraguaná Peninsula, PSB: Plato-San Jorge Basin, Q: Quetame Massif, RC: Raspas Complex, **SM**: Santander Massif, SNSM: Sierra Nevada de Santa Marta, SP: Sierra de Perijá, TI: Taos Island, UMV: Upper Magdalena Valley Basin, WC: Western Cordillera. Geology from Litherland et al. (1994) [17] and Gómez et al. (2007) [18].

The time period between ~414 and ~294 Ma is mainly amagmatic in Ecuador, Colombia and Venezuela although geographically restricted and small granitoids in the northern Cordillera Central of Colombia yield Carboniferous zircon U-Pb dates [19], and were interpreted by Leal-Mejia et al. 2019 [6] to have formed within an extensional environment focussed along the Otu-Pericos Fault (Figure 1). Spikings et al. 2021 [1] suggest that northwestern Gondwana was mainly a passive margin during this period, which is reflected as a paucity of Devonian-aged zircons in Carboniferous basins in Ecuador. However, Horton et al. 2010 [10] found a peak in Devonian-aged detrital zircons in Devonian sedimentary rocks in Colombia, leading them to conclude that a Devonian arc may have shed detritus into northwestern Gondwana, although the arc remains unidentified and it is possible that these zircons may be far travelled.

Geographically dispersed Permian intrusions define a now dismembered continental arc that started at ~294 Ma, although the igneous rocks within northwestern South America are poorly exposed relative to Ordovician, Triassic and younger units. Within Venezuela, Permian granitoids are only found in the Sierra de Perijá, Paraguana Peninsula ([2]) and the El Baul Massif [12] (Figure 1). The intrusions are more numerous within Colombia and crop out in the Sierra Nevada de Santa Marta (E.g. El Encanto Orthogneiss; [11,20]) and the central Cordillera Central (Colombia; Rovira Complex; [21,22]), whereas only a single Permian pluton has been found in Ecuador, which is located in the far southern Cordillera Real (Malacatos Complex [23,24]). These geographically dispersed occurrences are interpreted to have formed part of a now dismembered arc sequence that mainly formed on the conjugate margins to a Triassic rift within Gondwana [20,24,25], and is currently preserved intact in the Eastern Cordillera of Peru [14]. Alternatively, Vinasco et al. 2006 [26] suggests they formed during the Gondwana-Laurentia collision.

Permian magmatism was modified by prograde metamorphism with peak metamorphic conditions of ~770–830 °C and ~11.5–14 kb [11], which is best preserved in the Sierra Nevada de Santa Marta (Colombia), and is recorded in late Permian (254.0 ± 2.3 Ma–251.8 ± 3.8) migmatites in the relict conjugate margin (e.g., Chiapas Massif and Chortis Blocks [27,28]). Low grade metamorphism of the Diamante Fm. of the Santander Massif is considered to be Late Permian [29]. Metamorphism is interpreted to be a result of compression that accompanied terrane collision events [24,27], which also deformed most of the Permian rocks exposed in northwestern South America.

Triassic granodiorites and monzogranites are abundant in northwestern South America and within Colombia they are found in the Cordillera Central, the basement of the Plato–San Jorge Basin, the Sierra Nevada de Santa Marta and the Guajira Peninsula (Figure 1) [7,8,11,20–24,26,30–32]. Equivalent Triassic rocks in Ecuador are the Tres Lagunas Granite, Moromoro Granite and leucosomes of the Sabanilla Migmatite within the Cordillera Real and Amotape Complex of Ecuador [17,21,33–36]. Geochemical and isotopic characteristics are distinct from the Permian arc units, and unambiguously show they were mainly derived from melting pelitic rocks [24,36]. These acidic intrusions are part of a bimodal assemblage that includes amphibolitic (meta-gabbros/dolerites) dykes, sills and an ophiolitic sequence in the cordilleras Central and Real [21,22,26,36–38], all of which are depleted mantle melts that are variably contaminated with continental crust [36]. This Triassic bimodal igneous assemblage formed during continental rifting in a back-arc, and the arc is partially preserved in the conjugate margins (e.g., Mixteca Terrane, Oaxaquia, Maya Block; [24]). Early to middle Triassic U-Pb ages were also obtained from small granitic bodies in the Perijá Foothills, Toas Island (Figure 1), Merida Andes and a rhyolitic dyke in the Santander Massif [2], although the mafic end member has not been found in these regions and these may represent satellite intrusions distant to the primary rift axis.

Late Triassic–Jurassic igneous rocks are high-K calc-alkaline continental arc granitoids (Figure 1). The oldest units are undeformed exposures in the Mérida Andes [2,3] and the aerially expansive Santander Plutonic Group in the Santander Massif [2,5]. A younger, coherent belt of mainly unfoliated (local fault foliations), Pacific trench-parallel Jurassic batholiths are exposed along the length of the cordilleras Central and Real, and the Garzón Massif, (red colours in Figure 1; e.g., Ibagué and Abitagua batholiths) [7,21,36,39–44]. Similar aged, Jurassic batholiths are also found within the Sierra Nevada de Santa Marta [43,45]. Earliest Cretaceous granodioritic intrusions are significantly more foliated and these include the Azafrán Batholith in Ecuador (yellow colours in Figure 1) [36] and the Mariquita Stock in Colombia [41]. Further west, the continental arc sequence is represented by poorly dated mafic volcanic rocks along the western flanks of the Cordillera Real (Upano and Alao-Paute units) and Cordillera Central (Quebradagrande arc). The volcanogenic reworked sequences host detrital zircons and dense minerals that show they formed within continental crust [46]. The Alao Arc in Ecuador is faulted against anastomosed slivers of mafic–ultramafic rocks of the Peltetec Unit within the Peltetec Fault Zone (Figure 1), which are depleted mantle melts that formed during hyper-extension of the Early Cretaceous margin during ~145–112 Ma [36]. The Chaucha Block (Figure 1) was temporarily detached from the Early Cretaceous forearc during the same extensional event, and re-accreted at some time between 120–75 Ma [36]. Equivalent Early Cretaceous depleted mantle melts have not been found in Colombia.

3. Geochronological Characterisation

Geochronological analyses of the crystalline rocks in northwestern South America have been made since the late 1950's (e.g., [47–50]), and early attempts mainly used the K/Ar and Rb/Sr methods. The dates were usually interpreted as crystallisation ages, which lead to several tectonic reconstructions that have since shown to be incorrect. For example, a plethora of Carboniferous Rb/Sr and K/Ar dates from intrusions within the Mérida Andes lead Bellizia and Pimental (1994) [51] and Aleman and Ramos (2000) [52] to suggest that a Carboniferous arc formed on the Mérida Terrane, and that it had a Laurentian provenance and drifted from Laurentia to Gondwana prior to the amalgamation of Pangaea. However, more recent zircon U-Pb dates have shown that these intrusions form part of an Ordovician arc [2,3], leading to a revision in the tectonic reconstruction (see Section 6). Here we present a summary of crystallisation ages from northwestern South America, which are restricted to (i) zircon U-Pb concordia dates, and (ii) plateau $^{40}Ar/^{39}Ar$ dates when the rocks lack U-bearing phases (i.e., mafic units), and are interpreted with respect to the potential for excess ^{40}Ar, ^{40}Ar loss and $^{37,39}Ar$ recoil effects. K/Ar and Rb/Sr dates are entirely discarded, given the high mobility of the daughter isotopes, even in rocks that appear unaltered. The temporal distribution of 162 zircon U-Pb concordia dates are summarised in Figures 2 and 3, with 4 $^{40}Ar/^{39}Ar$ plateau (groundmass and plagioclase) dates from depleted mantle derived basalts and basaltic andesites. These dates are divided into specific groups according to time, field relationships and isotopic and geochemical characteristics.

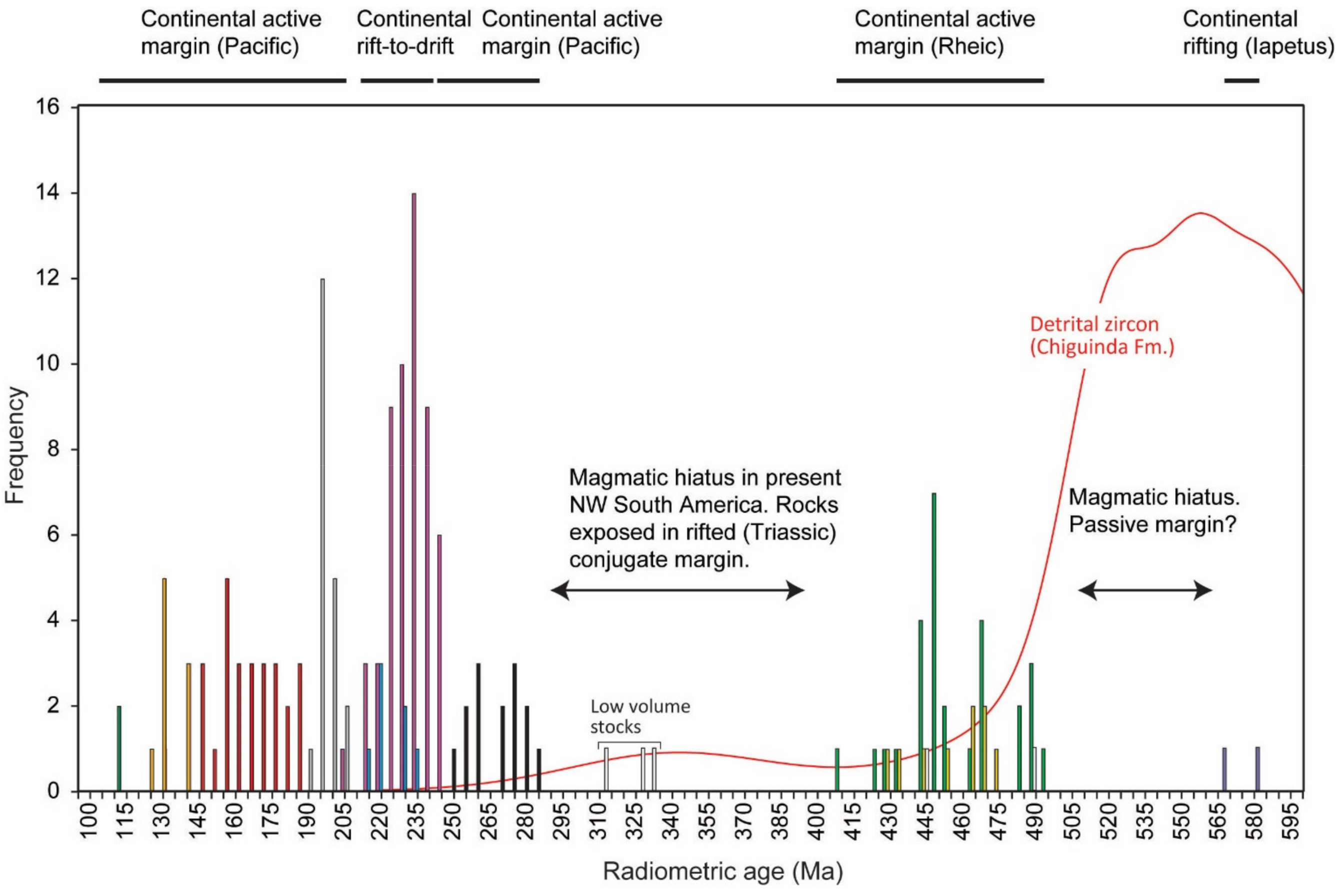

Figure 2. *Cont.*

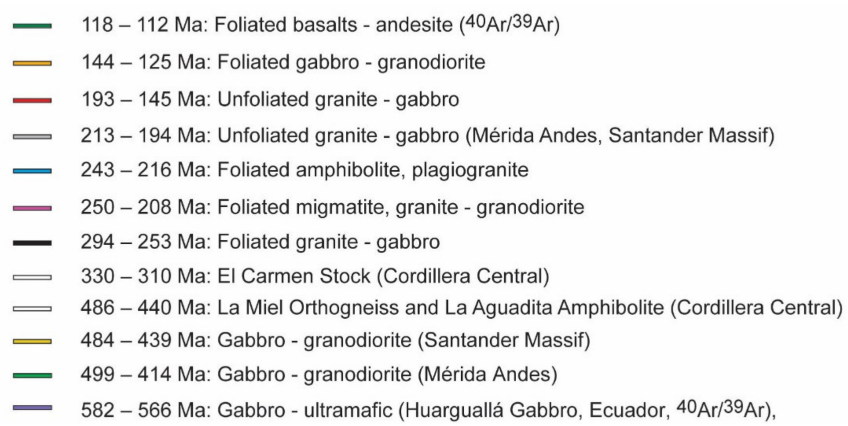

Figure 2. Histogram of crystallisation ages (mainly zircon ^{238}U-^{206}Pb concordia ages) of igneous rocks in Venezuela, Colombia and Ecuador during 499–112 Ma. Data are from Litherland et al. (1994) [17], Noble et al. (1997) [37], Vinasco et al. (2006) [26], Colmenares (2007) [45], Montes et al. (2010) [30], Weber et al. (2010) [31], Leal-Mejia (2011) [19], Restrepo et al. (2011) [32], Villagomez et al. (2011) [7], Mantilla-Figueroa et al. (2012, 2013) [4,5], Riel et al. (2013) [35], Cochrane et al. (2014a, b) [21,46], Martens et al. (2014) [8], Van der Lelij et al. (2016) [2], Bustamante et al. (2010, 2016, 2017) [22,40,41], Paul et al. (2018) [23], Rodriguez et al. (2018) [42], Piraquive et al. (2021) [11], Restrepo et al. (2021) [44], Spikings and Paul (2019) [24], Spikings et al. (2015, 2019, 2021) [1,36,43], Tazzo-Rangel et al. (2019; orthogneisses only) [3].

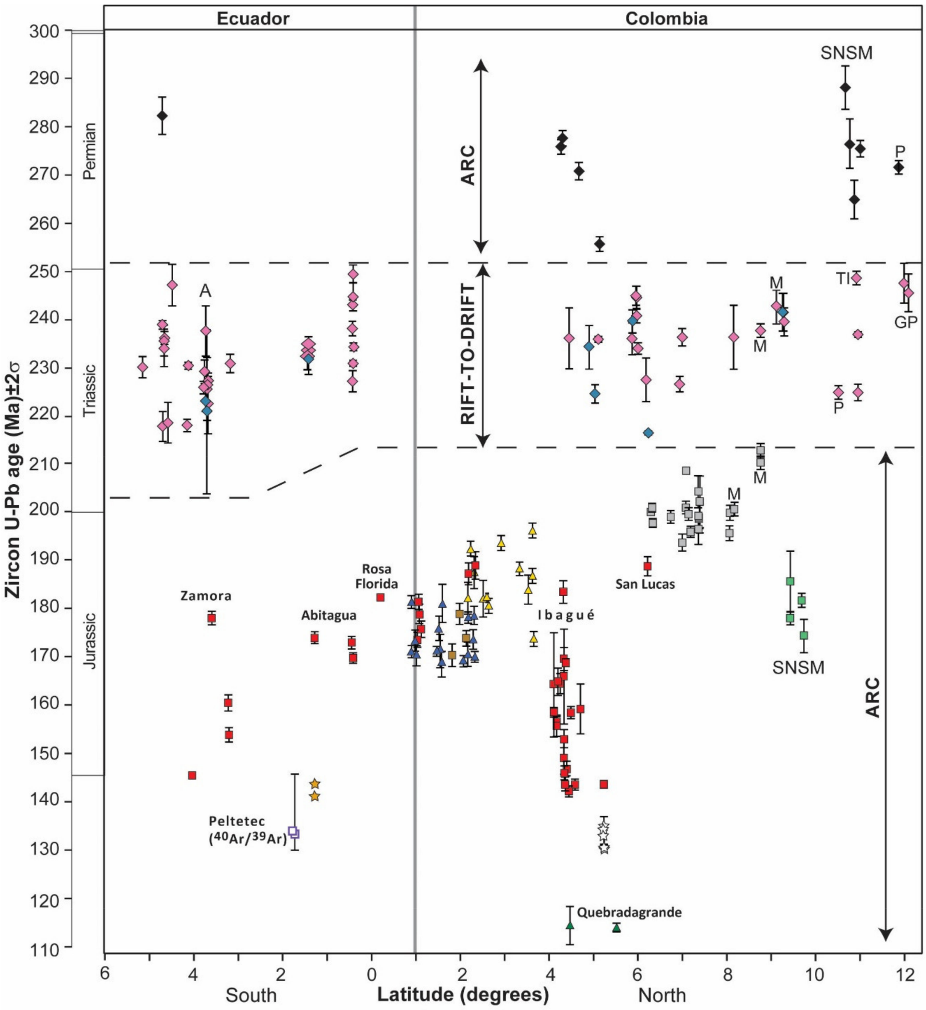

Figure 3. *Cont.*

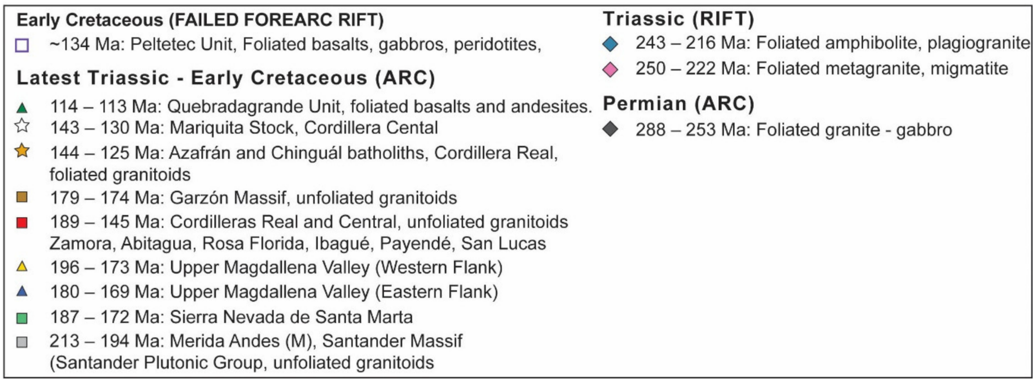

Figure 3. A comparison of crystallisation age (mainly zircon ^{238}U-^{206}Pb concordia ages) and latitude, showing the main arc and rift stages within northwestern South America. GP: Guajira Peninsula, SNSM: Sierra Nevada de Santa Marta, TI: Toas Island. Citations for dates are listed in the caption for Figure 2.

3.1. Late Neoproterozoic: Continental Rift

The first distinct group are two plateau $^{40}Ar/^{39}Ar$ dates (plagioclase) spanning between 582–566 Ma (623–531 Ma including 2 s uncertainties) from a gabbro and an ultramafic rock of the Huarguallá Gabbro, which are fault-bound slivers within the Peltetec Fault Zone of the western flank of the Cordillera Real in Ecuador (Figures 1 and 2) [1]. Neither zircon nor baddeleyite were found in these rocks and thus U-Pb dates were not obtained. The plagioclase do not contain excess ^{40}Ar or show evidence for $^{37,39}Ar$ recoil, and the plateau dates were interpreted by Spikings et al. (2021) [1] as accurate crystallisation ages, and are among the only Ediacaran-aged, depleted mantle derived melts that have been documented in northwestern South America. Mejia et al. (2012) [53] report a zircon U-Pb age of 577.8 $\pm$ 6.8/$-$9.0 Ma from a nepheline syenite located in an inlier in the Llanos Basin (Figure 1). These dates overlap with dates of syn-rift alkaline lava flows within the intra-continental, Puncoviscana Fold Belt in northwestern Argentina [54].

Tazzo-Rangel et al. (2021) [55] report U-Pb dates of detrital zircons in paragneisses of the Iglesias Complex in the Mérida Andes that are interpreted to constrain the maximum age of deposition of the protolith to 540–530 Ma.

3.2. Cambrian–Earliest Devonian: Continental Arc

Most Cambrian–Silurian magmatism is distal from the present-day Pacific and Caribbean margins (Figure 1). A distinct group of granitic-dioritic intrusions in the Mérida Andes (e.g., La Grita Diorite) and Santander Massif (e.g., Berlin Orthogneiss) yield zircon U-Pb concordia dates of 499–414 Ma and 484–439 Ma, respectively [2–5]. These overlap with the age of crystallisation of the protolith of the La Aguadita Amphibolites at 486–2.7/$-$14 Ma [9], and the La Miel orthogneiss in the Anacona Block of the Cordillera Central (Figure 1) [7,8], which yields U-Pb dates of 470–440 Ma, the Quetame (483 $\pm$ 19 Ma; La Mina granodiorite) [10] and Floresta massifs (464 $\pm$ 8 Ma; Otenga granite) [10], the Sierra Nevada de Santa Marta (449.7 $\pm$ 2.0 Ma) [11], the Caribbean Mountains of Venezuela (e.g., Choroni Granite; discordia intercepts), the El Baul Massif [12] and the Llanos Basin [13]. These Palaeozoic igneous units are not exposed in Ecuador, although they reappear in the northern Eastern Cordillera of Peru [14]. Tazzo- Rangel et al. (2021) [55] suggest that detrital zircons with U-Pb dates of ~530 Ma may be derived from a continental arc, and thus that magmatism may have started as early as 530 Ma, although the source rocks have not been identified. Peak upper amphibolite metamorphism in the Mérida Andes and Santander Massif occurred at ~472 Ma, and intrusions that are older than ~467 Ma are strongly foliated [2,3], suggesting a deformation phase occurred between 499–467 Ma. Garnet-bearing amphibolites of the La Miel orthogneiss were interpreted by Restrepo and Toussaint (1984) [15] and Bustamante and Juliana (2011) [16] to suggest it reached peak amphibolite facies within a subduction zone environment, although the timing of metamorphism is unclear. White mica yields a $^{40}Ar/^{39}Ar$ plateau date of 345 ± 2 Ma [26], which was interpreted by Vinasco et al. (2006) [26] as the timing of retrogression after amphibolite facies metamorphism, although this requires further validation because it could represent a mixed date between, for example, Ordovician and Triassic metamorphism.

3.3. Devonian–Carboniferous: Magmatic Hiatus

The time period between ~414 and ~296 Ma is mainly amagmatic in Ecuador, Colombia and Venezuela (e.g., [1,2,6]). An exception are geographically restricted and small Carboniferous tonalitic stocks in the northern Cordillera Central of Colombia (El Carmen stock; Figure 1) that yield three zircon U-Pb dates between 330–310 Ma [19] (Figure 2), and were interpreted by Leal-Mejia et al. (2019) [6] to have formed within an extensional environment focussed along the Otu-Pericos Fault (Figure 1). Very low volumes of magmatism during ~414 and ~296 Ma are reflected in a paucity of Devonian-aged detrital zircons in Carboniferous basins in Ecuador [1], Peru [56,57] and farther south (e.g., [58]). However, Horton et al. (2010) [10] found a small peak in Devonian-aged detrital zircons in Devonian sedimentary rocks in Colombia, although the primary source rocks have not been identified. Carboniferous detrital zircons (Figure 2) are found in low proportions in Carboniferous sedimentary units in Ecuador (Chiguinda Fm.) [1] and Colombia (Guatiquia Fm.) [10]. Felsic Triassic intrusions and leucosomes host a small proportion of zircon cores that yield Carboniferous U-Pb concordia dates, although many of these Triassic intrusions formed by melting Carboniferous pelites (Chiguinda Fm. of Ecuador) [1], and the zircons are considered to be sourced from southern latitudes (e.g., Carboniferous intrusions currently exposed in the Eastern Cordillera of Peru).

3.4. Permian: Continental Arc

Permian continental arc magmatism is recorded in northwestern Gondwana by intrusions that crystallised during 294–253 Ma (Figures 2 and 3), although the igneous rocks are highly geographically dispersed and dismembered. Within Venezuela, Permian intrusions are found in the El Baul Massif (294–283 Ma; [12]), and a diorite in the Paraguana Peninsula (272 ± 3 Ma; [2]). The intrusions are more numerous within Colombia and crop out in the Guajira Peninsula (272 ± 1.1 Ma; [59]), Sierra Nevada de Santa Marta (~288–264 Ma, El Encanto Orthogneiss and other mylonitised granites; [11,20]) and the central Cordillera Central where they are referred to as the Rovira Complex (~278–253 Ma, Colombia; [21,22,24]). In contrast, only a single Permian pluton has been found in Ecuador, which is located in the far southern Cordillera Real (~283 Ma; Malacatos Complex; [23,24]) close to the Peruvian border.

3.5. Triassic (250–208 Ma): Continental Rift

Triassic granodiorite and monzogranite leucosomes and variably foliated plutons are abundant in northwestern South America and they are described separate to the Permian intrusions because they are geochemically and isotopically distinct (see Section 4). Within Colombia they are found in the Cordillera Central (Cajamarca Complex), the basement of the Plato–San Jorge Basin, the Sierra Nevada de Santa Marta (La Secreta gabbro) and the Guajira Peninsula (e.g., Uray Gneiss; Figure 1), and yield zircon U-Pb concordia ages (Figures 2 and 3) ranging between 247.6 ± 4.1 Ma and 222 ± 10 [7,8,11,20–24,26,30–32,59]. The Tres Lagunas Granite, Moromoro Granite and leucosomes of the Sabanilla Migmatite within the Cordillera Real and Amotape Complex of Ecuador yield zircon U-Pb concordia dates that range between 249.9 ± 1.8 Ma and 207.6 ± 9.2 Ma [17,21,23,24,34–36,60]. These acidic intrusions in Colombia and Ecuador are part of a bimodal assemblage that includes amphibolitic (meta-gabbros-basalts) dykes, sills and an ophiolitic sequence in the cordilleras Central (e.g., Santa Elena Amphibolite) and Real (e.g., Piedras Amphibolite) that yield dates spanning between 243 ± 4 Ma and 216.6 ± 0.4 Ma [21,22,24,26,36–38]. Early to middle Triassic U-Pb ages were also obtained from small granitic bodies in the Perijá Foothills (225.1 ± 1.5 Ma) [2], Toas Island (248.9 ± 1.7 Ma; Figure 1) [2], Mérida

Andes (246–228 Ma) [2,3] and a rhyolitic dyke in the Santander Massif (250.7 ± 4.3 Ma) [2], although the mafic end member has not been found in these regions. The Triassic assemblage is interpreted to have formed during a continental rift-to-drift transition (see Section 6) [21,24,36].

3.6. Late Triassic–Jurassic (213–145 Ma): Unfoliated Intrusions of a Continental Arc

The Triassic rift sequence is frequently in faulted contact with a younger, late Triassic–Jurassic, calc-alkaline continental arc (Figure 1). The oldest sequence of Mesozoic continental arc igneous rocks are scattered and undeformed exposures of granites, granodiorite, tonalites and rhyodacites in the Merida Andes (Figures 2 and 3; 213–202 Ma; e.g. El Carmen granodiorite; [2]) and the aerially expansive Santander Plutonic Group in the Santander Massif (209–195 Ma; e.g. Onzaga granodiorite; [2,5]). A younger, coherent belt of mainly unfoliated (local fault foliations), Pacific trench-parallel Jurassic granitic (dominantly granodioritic) to gabbroic batholiths are exposed along the length of the cordilleras Central and Real, and the Garzón Massif, with dates spanning between 193–145 Ma (red colours in Figure 1; e.g., San Lucas and Ibagué batholiths in Colombia, Abitagua and Zamora batholiths in Ecuador; [7,19,36,39–44,46]). Acidic intrusions dominate exposure of the Sierra Nevada Block of the southern Sierra Nevada de Santa Marta (northern Colombia; Figure 1), and the few radiometric dates that exist include a Jurassic U-Pb (zircon) age of 179.6 ± 13.1 Ma [45], and Jurassic hornblende and biotite $^{40}Ar/^{39}Ar$ plateau dates that span between 187–172 Ma [43].

A comparison of zircon U-Pb age and latitude (Figure 3) suggests that the timing of the onset of magmatism may become younger from northern Colombia to southern Ecuador. The Jurassic intrusions of the Sierra Nevada de Santa Marta break this trend, which may reflect post-Jurassic displacement of these rocks from southern latitudes (e.g., [61]). However, this apparent trend may be an artifact of sampling density, given that it is not consistent with the large quantity of dates acquired from the Ibagué Batholith. A more robust chronological trend is seen when the crystallisation ages are compared with their distance from the equivalent Silvia-Pijao (Colombia) and Ingapirca-Peltetec (Ecuador) Faults (Figure 4), showing that latest Triassic-Jurassic magmatism generally becomes younger as it approaches the approximate location of the contemporaneous plate margin. Assuming insignificant strike-slip displacement, this implies that Jurassic magmatism initiated far from the trench at ~213 Ma, and these rocks are currently exposed within the Mérida Andes, Santander Massif (Figures 1 and 3) and in the southern Cordillera Central [19,44]. This older magmatic belt (>189 Ma) is not exposed, or did not form in Ecuador. Magmatism migrated westwards at ~194 Ma and stabilised within the region that is now exposed within the Cordilleras Central and Real, and along the flanks of the Upper Magdalena Valley, throughout the Jurassic [36,43].

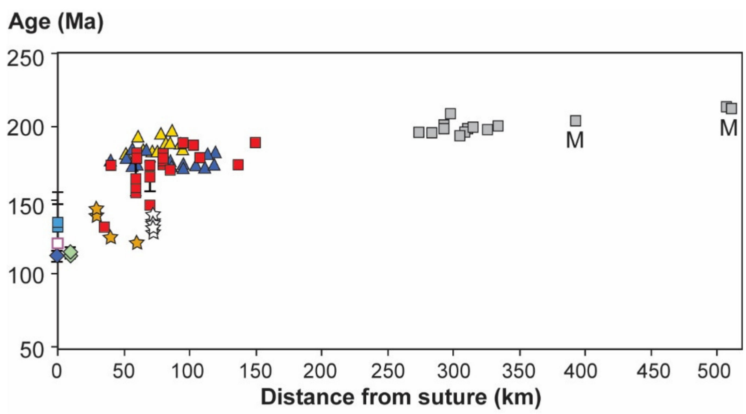

Figure 4. A comparison of crystallisation age (mainly zircon ^{238}U-^{206}Pb concordia ages) and present-day longitudinal distance from the palaeotrench, which is defined as the Ingapirca-Peltetec fault in Ecuador, and the Silvia-Pijao fault in Colombia. Symbols are the same as in Figure 3. M: Mérida Andes.

3.7. Early Cretaceous: Foliated Igneous Rocks of a Continental Arc

Younger dominantly granodioritic intrusions are significantly more foliated than the latest Triassic–Jurassic intrusions and these include the Azafrán and Chingual Batholiths in Ecuador (144–125 Ma; [36]) and the Mariquita Stock in Colombia (143–130 Ma; [41]). A meta-andesite of the Upano Fm. in the Cordillera Real yields a zircon U-Pb crystallisation age of 121.0 ± 0.8 Ma [46] and is considered to have been deposited in the pre-orogenic Salado Basin. These igneous units are more extensively exposed in Ecuador (yellow colour in Figure 1), and were generally located westward of the Jurassic igneous rocks (Figure 4), and thus were probably closer to the contemporary trench.

Further west, fault bounded continental arc sequences are represented by mafic volcanic rocks along the western flanks of the Cordillera Real (Upano and Alao-Paute units) and Cordillera Central (Quebradagrande arc). The volcanogenic reworked units host detrital zircons and dense minerals that show they formed within continental crust and were deposited after ~149 Ma (U-Pb detrital zircons; [46]). However, the basalts and basaltic andesites of the Alao-Paute unit have not been successfully dated, and $^{40}Ar/^{39}Ar$ plateau dates (~77–33 Ma) are severely compromised by secondary alteration and thus do not record the time of crystallisation [62]. Volcanic units in the Quebradagrande Arc yield zircon U-Pb dates of 118–112 Ma [7,46], which are consistent with the presence of Berriasian to Aptian fossils [63], and the date of a cross-cutting intrusion (93 ± 1 Ma; [64]). Toussaint and Restrepo (1994) [65] report a K/Ar (whole rock basalt) date of 105 ± 0.8 Ma, although it is likely to be at least partially reset.

Faulted slivers of greenschist grade meta-basalts and meta-gabbros within the Peltetec Unit along the western flanks of the Cordillera Real (Figure 1) yield plagioclase $^{40}Ar/^{39}Ar$ plateau dates of 134.7 ± 0.9 and 134.4 ± 13 Ma, which are interpreted as the minimum crystallisation ages of the protoliths [36]. These units do not record arc signatures, and are interpreted as depleted mantle melts that formed during hyperextension of the Early Cretaceous arc [36] (see below).

4. Geochemical and Isotopic Characterisation

4.1. Whole Rock Geochemical Compositions: Arcs

Whole rock major oxide, trace element and Rare Earth Element (REE) abundances of the granitic to dioritic intrusions that crystallised during 499–414 Ma, 294–253 Ma and 213–145 Ma (Figure 5A,B) are typical of continental arc rocks. These rocks (i) are not bimodal and have compositions dominated by granodiorites with smaller amounts of granites, diorites and gabbros, (ii) have calcic to alkali-calcic differentiation trends on the modified alkali-lime index of Peacock (1931) [66], (iii) are mildly peraluminous to metaluminous with ASI values that span between ~1.2–0.6 (Figure 5D), (iv) are enriched in Light Ion Lithophile Elements (LILE), and (v) have N-MORB normalised negative Nb, Ta and Ti anomalies. Furthermore, tectonic discrimination based on (La/Sm)n v Nb/La places these units within the continental arc field (Figure 5E). Some variations occur between and within these three time periods, and these are discussed in more detail elsewhere (e.g., [36]). For example, within the group of mainly unfoliated Late Triassic–Jurassic (213–145 Ma) intrusions, the Late Triassic–Early Jurassic granitoids within the Mérida Andes and Santander Massif are the most enriched in LILE. Early Cretaceous dacites, andesites, basalts and gabbros of the Quebradagrande (Colombia) and Alao (Ecuador) sequences are mainly metaluminous and span a larger range in Aluminium Saturation Index than the Cambrian–Earliest Devonian and Early Triassic–earliest Cretaceous intrusions. Unsurprisingly, they are more depleted than the older granitoids, although they also yield negative Nb, Ta and Ti anomalies that are characteristic of arc rocks. Tectonic discrimination using (La/Sm)n v Nb/La (Figure 5E) places these in an oceanic arc field, although this is not consistent with detrital zircons in the associated volcanogenic sedimentary units that have a Gondwanan continental age distribution and they are interpreted to be mildly differentiated continental arc units [36] (see Section 6).

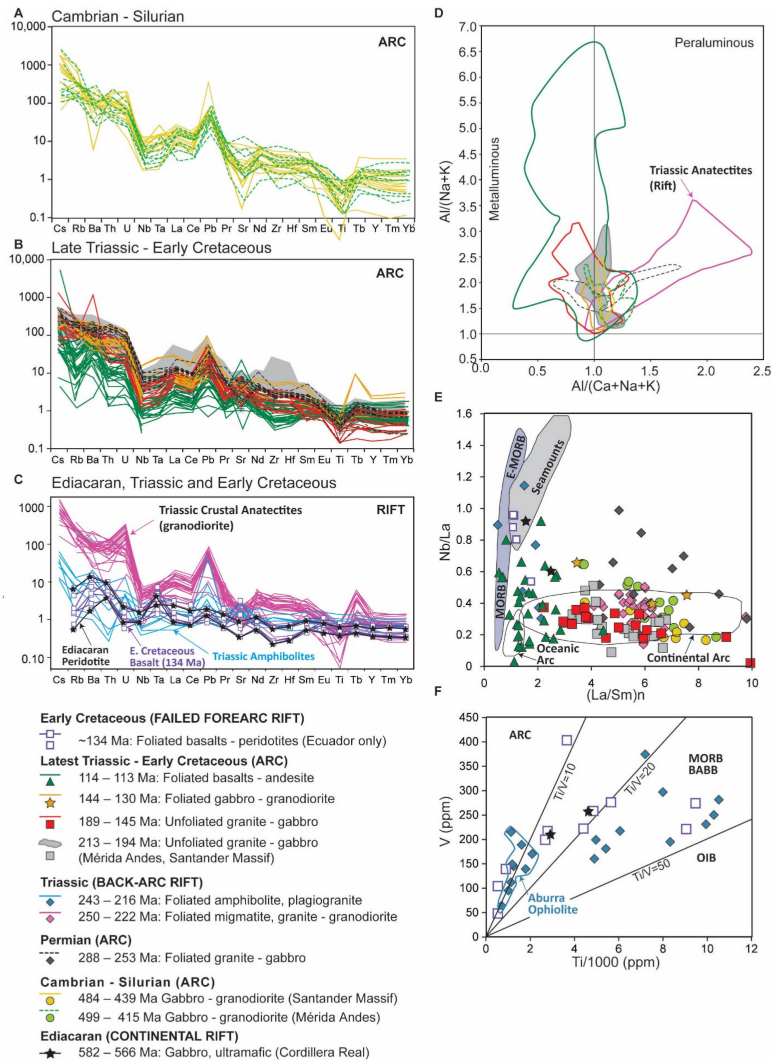

Figure 5. Summary whole rock geochemical data from igneous rocks that crystallised during 499–112 Ma in Venezuela, Colombia and Ecuador. (**A**) Cambrian–Earliest Devonian continental arc intrusions that are exposed in the Mérida Andes and the Santander Massif. (**B**) Permian–Early Cretaceous continental arc intrusions that are mainly exposed in the Sierra Nevada de Santa Marta and the cordilleras Central and Real, showing a gradual depletion towards younger rocks. (**C**) Late Neoproterozoic, Triassic (felsic and mafic end members) and Early Cretaceous rift. (**D**) discrimination between peraluminous and metaluminous rocks using Al, Ca, Na and K [67] showing the highly peraluminous nature of the Triassic, rift-related crustal anatectites. (**E**) Discrimination between depleted mantle (MORB, E-MORB) and arc settings for all of the dated units (499–112 Ma) using (La/Sm)n v Nb/La [68]. (**F**) Discrimination between arc and extensional settings using Ti and V [69]. Data are from Litherland et al. (1994) [17], Nivia et al. (2006) [63], Martinez et a. (2007) [38], Bustamante et al. (2010) [40], Villagomez et al. (2011) [7], Rodriguez and Zapata (2013) [70], Cochrane et al. (2014a, b) [21,46], Vinasco et al. (2006) [26], Van der Lelij et al. (2016) [2], Rodriguez et al. (2018) [42], Spikings et al. (2015, 2021) [1,36].

4.2. Radiogenic and Stable Isotopic Compositions: Arcs

The oldest arc units (plutons with dates spanning between 499–414 Ma) exposed in the Mérida Andes and the Santander Massif yield whole rock εNdi values (Figure 6A) ranging between −8.71 and 3.06 [71], while present day whole rock Pb isotopic compositions (Figure 6B) vary between 18.628–20.944 ($^{206}Pb/^{204}Pb$), 15.643–15.854 ($^{207}Pb/^{204}Pb$) and 38.556–40.568 ($^{208}Pb/^{204}Pb$), and stable oxygen isotopes in quartz ($d^{18}O$; Mérida Andes only) vary between 9.03–14.27 (Figure 6D). εHft (zircon) values (average values from a single rock with indistinguishable values from single ablation spots) from Cambrian–Earliest Devonian magmatic or metamorphic rims range between −10.40 ± 0.53 and 5.26 ± 0.44 [3,71], which correspond to Lu-Hf model ages of ~1.7 to ~0.80 Ga (Figure 6C). There are no clear differences in the isotopic compositions of Palaeozoic arc intrusions in the Mérida Andes and the Santander Massif. No similar isotopic data have been published from Ordovician igneous units in the Cordillera Central (e.g., Le Miel orthogneiss). The εHft (zircon) values from the older, foliated plutons (499–467 Ma) are <−5, whereas the younger rocks trend towards more radiogenic compositions. Similarly, foliated granitoids with zircon U-Pb ages between 499–467 Ma have the least radiogenic compositions with εNdi values spanning from −3.22 to −7.15, which are among the least radiogenic data within all of the arc igneous rocks in northwestern South America. Granitoids that crystallised during ~467 and ~414 Ma have more radiogenic εNdi values with a maximum of 1.58 ± 0.05. The present day $^{206}Pb/^{204}Pb$ and $^{207}Pb/^{204}Pb$ ratios (Figure 6B) are more radiogenic than the terrestrial Pb evolution curve of Stacey and Kramer (1975) [72] and overlap data obtained from the Guyana Shield in southern Venezuela, the Garzón Massif in Colombia and the Amazonian Craton in western Brazil. These contrast with present day Pb isotopic compositions from Laurentian cratonic rocks or the Laurentia-derived Cuyania Terrane [73], which are less radiogenic than the curve of Stacey and Kramers (1975) [72]. A comparison of $d^{18}O$ (quartz; Mérida Block only) with zircon U-Pb date yields no clear relationship, and $d^{18}O$ straddles both the S- and I-type fields of Harris et al. (1997; Figure 6D; [74]).

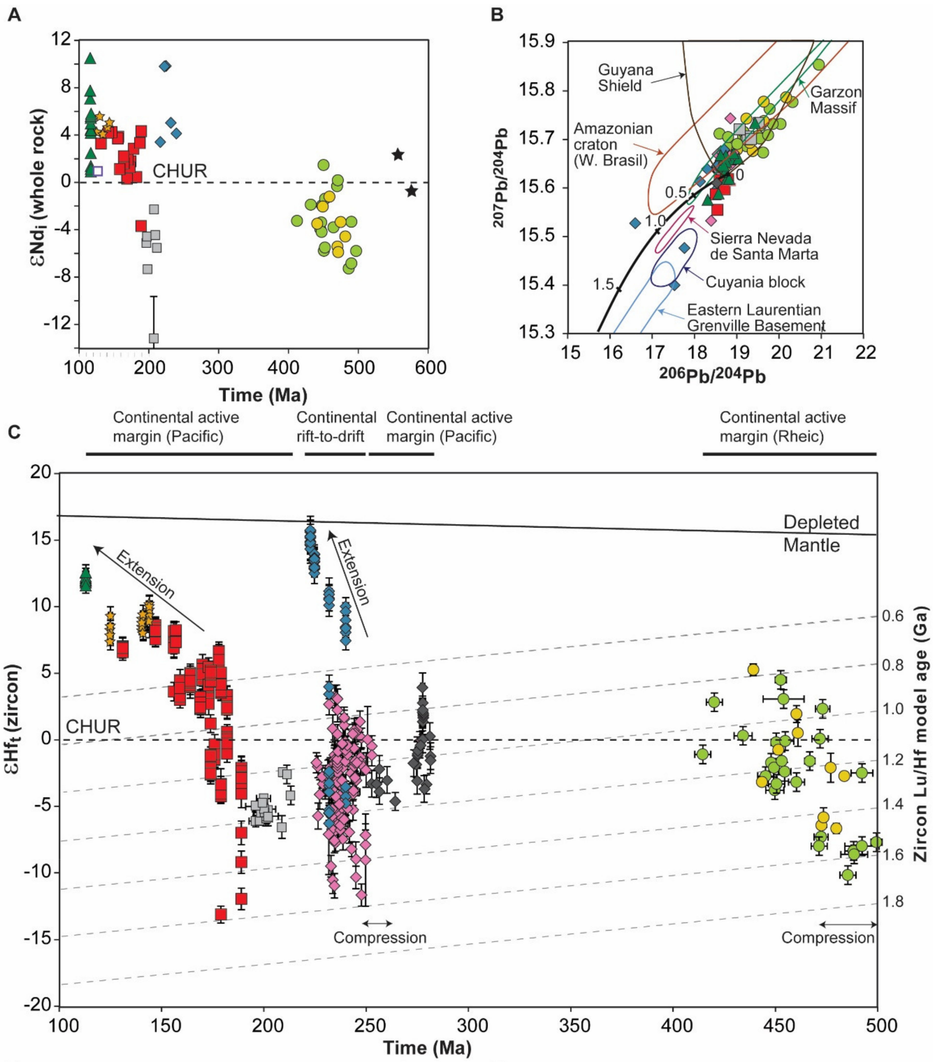

Figure 6. *Cont.*

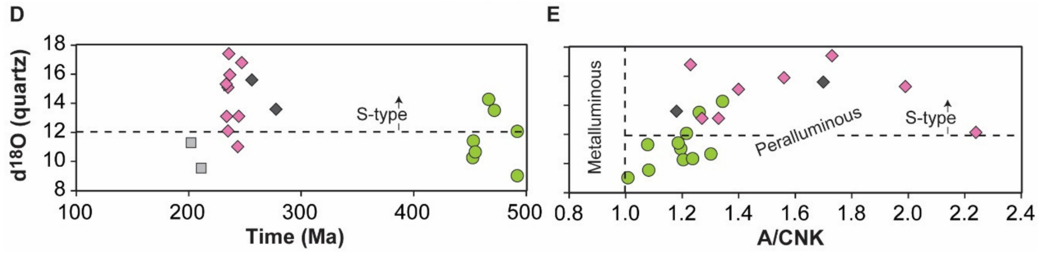

Figure 6. Summary isotopic compositions of igneous rocks that crystallised during 499–112 Ma in Venezuela, Colombia and Ecuador. (**A**) whole rock Nd, (**B**) uncorrected whole rock and feldspar (Triassic only) Pb isotopic compositions showing fields (uncorrected data) for major basement regions in Colombia [75] and western Gondwana and Laurentia [76]. The black line shows the terrestrial evolution trend [72]. (**C**) Hf isotopic compositions of magmatic rims of zircons showing the corresponding two-stage Lu-Hf model ages (calculated using a $^{176}Lu/^{177}Hf$ ratios of 0.0113 and 0.0384 for average and juvenile continental crust, respectively; [77]) and highlighting periods of compression and extension. (**D**,**E**) Comparisons of d^{18}O (quartz) with time (zircon ^{238}U-^{206}Pb concordia age) and Aluminium Saturation Index (A/CNK) highlighting the S-type field of Harris et al. (1997) [74]. Data are from Ordoñez-Carmona et al. (2006) [78], Mantilla-Figueroa et al. (2012) [4], Cochrane et al. (2014a, b) [21,46], Bustamante et al. (2016, 2017) [22,41], Van der Lelij et al. (2016, 2019) [2,71], Paul et al. (2018) [23], Spikings et al. (2015, 2021) [1,36], Tazzo-Rangel et al. (2019; orthogneisses only) [3]. Symbols are the same as in Figure 5.

Fewer isotopic data have been obtained from the Permian arc granitoids. Single ablation spots in zircons that gave Permian U-Pb dates from three foliated granites (Cordillera Central, Colombia) yield single ablation spot values of εHft ranging between −6.3 and 4.0 (Figure 6C), with weighted averages between −3.45 ± 0.40 and 1.96 ± 0.31 [21]. Despite the fact that these data were only obtained from three rocks, a distinct group of younger Permian spot dates (260–250 Ma) yield the least radiogenic εHft values. Lu-Hf model ages for the Permian intrusions range between ~1.2 and ~0.7 Ga (Figure 6C). Pb isotopic compositions have only been obtained from feldspar extracted from a single Permian granite of the Malacatos Unit (southern Cordillera Real, Ecuador; [23]), and yield present day values (feldspar) of 18.560 ± 0.001 ($^{206}Pb/^{204}Pb$) and 15.61 ± 0.001 ($^{207}Pb/^{204}Pb$), which lies within the cloud of present day whole rock Pb isotopic compositions obtained from Triassic crustal anatectites (rift) and latest Triassic–Early Cretaceous intrusions (arc). Finally, d^{18}O (quartz) data from two Permian granitoids of the Cordillera Central yield crustal values of 13.6 ± 0.2 and 15.6 ± 0.2 (Figure 6D,E; [21]), which are typical of S-type granites [74], and overlap with the most crustal values obtained from the Cambrian–Earliest Devonian intrusions (arc), while they are similar to the Triassic leucosomes and granodiorites (rift).

Unfoliated (local fault foliation) Late Triassic–Jurassic granitoids yield clear temporal trends in Nd (whole rock) and Hf (zircon) isotopic compositions. Whole rock εNdi values from the older, Late Triassic–earliest Jurassic intrusions in the Mérida Andes and the Santander Massif (213–194 Ma) show the least radiogenic compositions and range between −13.06 and −2.16 (Figure 6A), and are similar to most of the Cambrian–Earliest Devonian granitoids that are exposed in the same two regions (Figure 1). Younger Jurassic granitoids exposed in the cordilleras Central and Real and the Garzón Massif (193–145 Ma) yield more radiogenic εNdi (whole rock) values and range from −6.00 to 9.25, and the Nd isotopic composition becomes more radiogenic as the rocks become younger. The εHft (zircon) data reveal the same trend (Figure 6C), where single ablation spot values in the Mérida Andes and Santander Massif (213–195 Ma) range from −6.11 to −2.46, whereas the younger granitoids (193–145 Ma) yield εHft (zircon) values that progressively increase from −7.00 to 8.60 through the Jurassic. Present day Pb isotopic compositions straddle the terrestrial Pb evolution curve of Stacey and Kramer (1975) [72], and extend to less radiogenic values than the Cambrian–Earliest Devonian arc rocks (Figure 6B).

The younger, pervasively foliated Early Cretaceous granodioritic intrusions (144–125 Ma; Azafrán and Chinguál Batholiths in Ecuador; Mariquita Stock in Colombia) yield εNdi (whole rock) that span between 4.1 and 5.6, and weighted mean (single hand specimens) εHft (zircon) values between 7.89 ± 0.71 and 9.40 ± 1.30. These values are more radiogenic than the undeformed Jurassic intrusions, and are consistent with the Jurassic trend towards depleted mantle compositions in younger rocks.

Finally, mafic volcanic rocks from the Early Cretaceous Quebradagrande arcs yield εNdi (whole rock) values spanning between 2.59 and 10.49 (Figure 6A; [46]). However, not all of these units have been dated, and these initial values have been determined for an age of 113 ± 1 Ma [7,46], which was obtained from two basalts of this sequence. Basalts to andesites of the Alao arc (Ecuador) yield extremely similar εNdi (whole rock) values that lie between 2.59 and 10.49 [46], which were determined assuming a crystallisation age of 121 ± 0.8 Ma (zircon U-Pb age of metagabbros of the Upano unit; [46]). εHft (zircon) values have only been obtained from a single rock of the Quebradagrande Unit (no non-reworked zircon has been identified in the Alao arc; Figure 6C), and give a value of 12.11 ± 0.17 [46]. The Nd and Hf isotopic compositions also continue the same late Triassic–Jurassic trend towards progressively more radiogenic source regions. Present day whole rock Pb isotopic compositions (Figure 6B; [46]) range between 18.3137–19.4336 ($^{206}Pb/^{204}Pb$), 15.5751–15.7337 ($^{207}Pb/^{204}Pb$) and 37.9673–39.1759 ($^{208}Pb/^{204}Pb$), and thus they are less radiogenic than the Cambrian–Earliest Devonian intrusions, although they are extremely similar to values obtained from the latest Triassic-Jurassic arc units, and the Triassic rift-related rocks

4.3. Whole Rock Geochemical Compositions: Rifts

Ultramafic and mafic (mainly metamorphosed basalts and gabbros) dykes and sills that formed during 582–566 Ma (Huargualla Gabbro Unit; [1]), 243–216 Ma and at ~134 Ma (Peltetec Unit; [36]; Figure 1) yield whole rock geochemical compositions that are consistent with depleted mantle that has been contaminated by continental crust to varying degrees. N-MORB normalised trace element abundances of gabbros and basalts from all three time periods (Figure 5C) are similar and reveal slight enrichments in LILE and a lack of significant Nb, Ta and Ti anomalies associated with dehydration of a subducted slab, or significant contamination with a metasomatised continental lithospheric mantle, supporting an origin within the asthenosphere. As expected, a single sampled Ediacaran peridotite of the Huarguallá Gabbro is more depleted than the gabbro. A comparison of (La/Sm)n and Nb/La places these mafic rocks from all time periods (Figure 5E) within the E-MORB and transitionary fields, which is consistent with a lack of evidence for subduction of oceanic lithosphere. The Ediacaran and Triassic amphibolitic dykes, along with some basalts of the Peltetec unit (~134 Ma) are highly enriched in Ti relative to V (Figure 5F), and plot in the MORB or back arc basin basalt (BABB) field of Shervais (1982) [69]. However, the massive metagabbros of the Aburrá Ophiolite (El Picacho metagabbros; [38]) that yield very low K_2O abundances of 0.02–0.12 wt%, and the highly depleted ultramafic component of the Peltetec unit plots closer to the arc field, albeit in a region where the discriminatory power of Ti/V is low.

The Triassic amphibolites (meta-basalts and gabbros; 243–216 Ma) are temporally accompanied (250–208 Ma) by monzonites and granodiorites that form variably foliated plutons and are mainly exposed in the cordilleras Real and Central. Field observations show that these felsic rocks occur as leucosomes that formed by melting Carboniferous metapelites (in the Cordillera Real), and also as plutons. These felsic rocks follow a high-K calc-alkaline trend, and negative Nb, Ta and Ti anomalies are present (Figure 5C), which are typical of upper continental crust. Slight negative N-MORB normalized Ba, Eu, Sr and Ti anomalies suggest that plagioclase and Fe-Ti oxides have fractionated, and a positive Pb anomaly is probably derived from a protolith within the continental crust. These characteristics are similar to the arc igneous units, although the Triassic granitoids are highly peraluminous (ASI 1.05–2.38) compared to all other igneous units (Figure 5D).

4.4. Radiogenic and Stable Isotopic Compositions: Rifts

Isotopic tracing of the sources of the rift-related Huarguallá Gabbro (582–566 Ma; Cordillera Real, Ecuador) is limited to whole rock εNdi values of −0.57 and 2.40 (Figure 6A; [1]), which are similar to values (0.6 to 1.3) obtained from a similarly aged dyke complex (Egersund Dyke Complex, ~616 Ma; [79]) in Scandinavia, the relevance of which is discussed in Section 6.

Abundant isotopic data have been acquired from the Triassic bimodal rift-to-drift sequence. Whole rock Nd isotopic data have only been obtained from the amphibolites (243–216 Ma; meta- basalts/gabbros), and εNdi span between 4.13 and 10.18, and thus include some of the most juvenile compositions of the Phanerozoic igneous rocks that are comparable with some basalts of the Early Cretaceous arc (Figure 6A). εHft (zircon) compositions of single ablation spots of Triassic igneous and metamorphic rims (and xenocrystic cores) of zircons from the felsic anatectites (mainly granodiorites) span a large range of −11.7 ± 0.8 to 3.2 ± 0.9, and single spot values frequently span ~9 epsilon units within the same hand specimen (Figure 6C). These crustal values corroborate high $d^{18}O$ (quartz) values of 12.1 ± 0.2 to 17.4 ± 0.2, which fall within the S-type field of Harris et al. (1997; Figure 6D,E; [74]). The large range in εHft (zircon) values is considered to reflect the heterogeneous nature of the crustal source regions [21,24,36]. Five amphibolites yield a large range of εHft (zircon) compositions from single ablation spots of Triassic igneous and metamorphic rims that span between −6.3 ± 0.8 and 15.7 ± 0.8 [21,22], overlapping with depleted mantle compositions (Figure 6C). The oldest three of these amphibolites (239–231 Ma) yield a large range of εHft values showing that zircons are derived from both crustal, non-radiogenic and juvenile εHft source regions. However, the youngest two amphibolites (225–223 Ma) only contain zircons with radiogenic εHft compositions (mean values of 13.31 ± 0.25 and 15.00 ± 0.29). Lu-Hf model ages for Triassic zircons within the Triassic crustal anatectites range between 0.89–1.4 Ga, which overlap with model ages from the least radiogenic zircons in the oldest amphibolites. Present day Pb isotopic compositions of the Triassic monzogranites of the Cajamarca Complex (Colombia) and Tres Lagunas Granite (Ecuador; Figure 6B; [21,23]) overlap with the Jurassic–Early Cretaceous arc rocks. However, the Triassic amphibolitized mafic intrusions yield relatively un-radiogenic compositions ($^{206}Pb/^{204}Pb$ 18.53–18.51) and reveal a mixing array between the highly peraluminous crustal anatectites and depleted mantle during 239.7 ± 2.4 Ma and 216.6 ± 0.4 Ma.

Basalts and gabbros of the Peltetec unit that yield E-MORB signatures are considered to be the youngest Mesozoic rift-related sequence in Ecuador, although isotopic tracing information is limited to a metabasalt and a gabbro that yield εNdi (whole rock; Figure 6A) values of 1.21 and 1.17 [36].

5. Thermochronology

A very large quantity of thermochronological data have been obtained from north-western South America, including, in order of ascending temperature of partial daughter isotope loss, (U-Th)/He (apatite), fission track (apatite, zircon), $^{40}Ar/^{39}Ar$ (K-feldspar, muscovite) and U-Pb (apatite) data. A majority of these data yield Tertiary dates that were reset during or after the collision and accretion of the Caribbean Large Igneous Province along the Cauca-Almaguer (Colombia)–Ingapirca-Peltetec Fault (Ecuador). This study focusses on those data that constrain thermal histories prior to and during the collision of the Caribbean Large Igneous Province at ~75 Ma [80,81].

5.1. Cambrian-Carboniferous Constraints

The use of $^{40}Ar/^{39}Ar$ data to constrain t-T information is highly contentious [82], and published t-T paths should be viewed with caution. Regardless, three Ordovician intrusions (08VDL27, 32 and 41) in the central and southern Mérida Andes (proximal to the Caparo-Soledad Fault; Figure 1) yield $^{40}Ar/^{39}Ar$ muscovite plateau dates ranging between 379.6 ± 1.5 Ma and 353.4 ± 1.2 Ma [83]. The interpretation of these dates is ambiguous although they are similar to a muscovite $^{40}Ar/^{39}Ar$ plateau date of 345 ± 2 Ma [26] obtained from the Ordovician La Miel orthogneiss (Cordillera Central), which was interpreted by Vinasco et al. (2006) [26] as the timing of retrogression after amphibolite facies metamorphism. However, this interpretation requires further validation because they could also represent mixed dates between, for example, Ordovician and Permian or Triassic metamorphism. No Carboniferous $^{40}Ar/^{39}Ar$ dates have been obtained from the Santander Massif, although a Palaeozoic intrusion (zircon U-Pb 479.8 ± 3.1 Ma; [2]) yields a plateau muscovite $^{40}Ar/^{39}Ar$ date of 407.4 ± 1.4 Ma [83]. Regardless of the ambiguity surrounding the thermochronological interpretation of $^{40}Ar/^{39}Ar$ data, these dates suggest that the current surfaces of the southern Mérida Andes and the eastern Santander Massif were not heated to T > 400 °C after the Carboniferous.

5.2. Permian-Mesozoic Constraints

Apatite U-Pb dates (both bulk ID-TIMS and in-situ LA-MC-ICPMS) have been obtained from (i) an Ordovician granodiorite exposed in the Mérida Andes (zircon U-Pb 466.8 ± 2.5 Ma; [2]), and (ii) numerous Triassic felsic anatectites that are exposed along the lengths of the cordilleras Real and Central. First, the Ordovician granodiorite yields $^{238}U/^{206}Pb$ bulk dates (ID-TIMS) ranging between 251.9 ± 7.7 Ma and 265.9 ± 7.1 Ma, while larger grains yield older dates, supporting an interpretation that Pb was lost by volume diffusion assuming the existence of a single, grain scale diffusion domain. The best-fit t-T model for these data suggest this rock cooled rapidly (>4.5 °C/My) from >500 °C at ~260 Ma to <360 °C at ~250 Ma [83].

Apatite $^{238}U/^{206}Pb$ bulk (ID-TIMS) dates from the Triassic (rift) anatectites in Ecuador and Colombia span between 227–42 Ma, and become younger from northern Colombia to southern Ecuador [23]. Apatite $^{238}U/^{206}Pb$ dates from the Cajamarca Complex in the northern Central Cordillera, and Triassic granitoids in the northern Cordillera Real of Ecuador are 10–40 My younger than their zircon U–Pb dates, reflecting rapid cooling through 550–380 °C in the Triassic, and no subsequent re–heating to temperatures >380 °C (Figure 7A; [23]). In contrast, a majority of $^{238}U/^{206}Pb$ dates from Triassic anatectites in the southern Cordillera Real (south of 2°S) are younger than 100 Ma. Numerical modelling suggests that these Triassic rocks also cooled rapidly through 550–380 °C at various times during the Triassic, although they were re–heated to >380 °C in the Early Cretaceous (Figure 7B; [23,43,84]). $^{40}Ar/^{39}Ar$ muscovite plateau dates [23] and low temperature thermochronometers [85] support the accuracy of the t–T paths obtained from the apatite U-Pb data from both regions (Figure 7A,B).

Alkali feldspar plateau $^{40}Ar/^{39}Ar$ dates from the Jurassic Ibagué Batholith south of the Ibagué Fault (central Cordillera Central; Figure 1) span between 138–130 Ma [86], and temporally coincide with a region-wide angular unconformity in the Upper Magdalena Valley Basin in Colombia [87], the Oriente Basin in Ecuador [88] and in northern Peru [89], and were interpreted by Villagomez and Spikings (2013) [86] to record a distinct period of cooling driven by extension (“iv” in Figure 7A). The same extensional event is considered to be responsible for heating (via burial and increased heat flow) of the Triassic basement in southern Ecuador to T > 380 °C (Figure 7B). A younger group of alkali feldspar plateau $^{40}Ar/^{39}Ar$ dates from the Jurassic Ibagué Batholith were obtained from the north of the Ibagué Fault, where they span between 114–110 Ma [86]. These temporally coincide with deposition of the upper Aptian to middle Albian, fluvial–estuarine Caballos Fm. that is exposed in the Upper Magdalena Valley Basin [90]. Dense mineral assemblages and detrital zircon FT dates suggest that this sequence, along with equivalent rocks in Ecuador (Hollín Fm.) were partly derived from a proto-Cordillera that was exhuming in the Early Cretaceous [91,92], and the $^{40}Ar/^{39}Ar$ dates are interpreted to reflect rock a period of rapid cooling (point ‘iii’ in Figure 7A) driven by rock uplift and erosion [86].

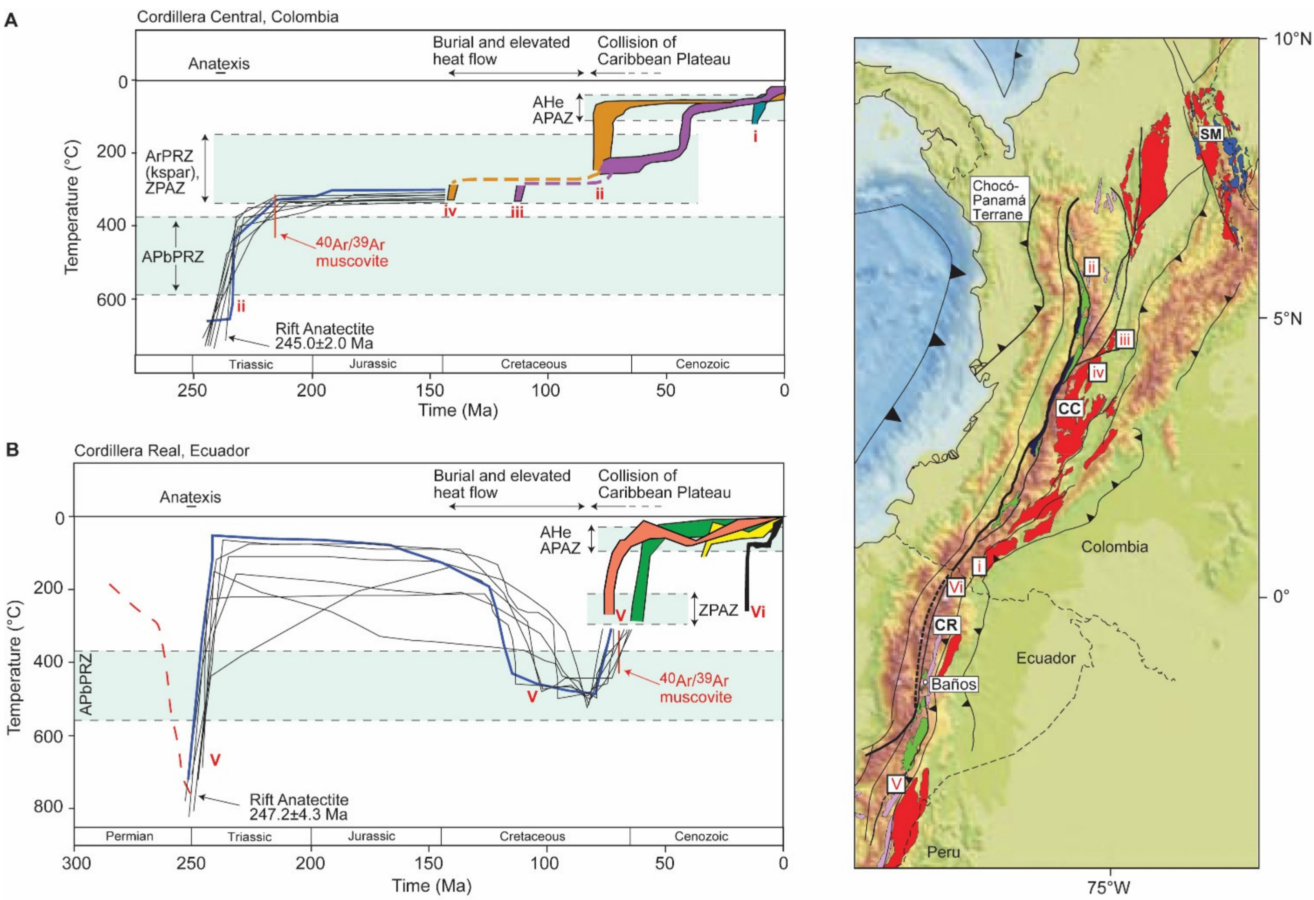

Figure 7. Thermochronological data obtained from Triassic and younger crystalline from (**A**) northern Colombia, and (**B**) southern Ecuador. Time-Temperature solutions have been obtained from (i) apatite U-Pb dates obtained for Triassic felsic crustal anatectites (black lines, blue line is the best-fit), (ii) $^{40}Ar/^{39}Ar$ muscovite (Ecuador and Colombia; vertical red bars) and alkali feldspar (Colombia only, proximal to the Ibagué Fault; solid envelopes) data, and (iii) zircon and apatite fission track and (U-Th)/He data (Colombia and Ecuador; solid envelopes). Solutions are only shown for the cordilleras Real and Central. Plateau muscovite $^{40}Ar/^{39}Ar$ dates overlap with the t-T solutions obtained from the apatite U-Pb data. Modelling details and data are provided in Spikings et al. (2010) [85], Cochrane et al. (2014) [84], Paul et al. (2018) [23] and Spikings and Paul (2019) [24]. Labels i to vi on the thermal history solutions and the map show the geographic distribution of cooling and heating. AHE: Apatite He Partial Retention Zone, ArPRZ: Ar Partial Retention Zone in K-feldspar, APAZ: Apatite Partial Annealing Zone, APbPRZ: Apatite Pb Partial Retention Zone, ZPAZ: Zircon Partial Annealing Zone.

$^{40}Ar/^{39}Ar$ (hornblende and biotite; Ecuador only), and zircon and apatite fission track data from mainly Triassic and Jurassic granitoids reveal a distinct period of rapid cooling during 80–70 Ma in the Antioquia region of the Cordillera Central (point 'ii' in Figure 7A; [86]), and the southern Cordillera Real (point 'v' in Figure 7B; [80,85]), although it is likely that most rocks exposed within the Cordilleras Central and Real experienced rapid cooling during this period [85]. The same cooling event is recorded in the apatite U-Pb data obtained from Triassic anatectites in southern Ecuador (Figure 7B; [23,84]). Similarly, Villagomez et al. (2011) [93] report apatite fission track data from the Sierra Nevada de Santa Marta (northern Colombia; Figure 1) that suggest the southern regions of that faulted block cooled rapidly during 65–58 Ma.

6. Tectonic Synthesis Based on the Geochemical and Isotopic Data

6.1. Late Neoproterozoic

Late Neoproterozoic gabbros and ultramafic rocks of the Huargualléa Gabbro occur in anastomosed slivers of the Peltetec Fault Zone in Ecuador, which separates Jurassic quartzites and slates of the continental Chaucha Block from the Alao Arc (Figure 1). In addition, a single nepheline syenite in the Llanos Basin of Colombia yields a zircon U-Pb age of 577.8 ± 6.8/−9.0 Ma [53]. The Huargualléa Gabbro crystallised during 623–531 Ma (including the 2σ uncertainties of $^{40}Ar/^{39}Ar$ dates), and were derived from an asthenospheric source that has been contaminated by ~25% of continental crust [1]. These rocks are coeval with syn-rift alkaline lava flows that are intercalated within the intra-continental, Puncoviscana Fold Belt in northwestern Argentina that formed during rift-drift tectonics during ≥600–535 Ma [54], and mafic intrusions, carbonatites and kimberlites that collectively form the Central Iapetus Magmatic Province within Scotland, Scandinavia and North America (e.g., [94,95]). Furthermore, a comparison of the elemental and Nd isotopic compositions of the Scandinavian and Egersund Dyke complexes (Norway) with the Huargualléa Gabbro unit suggests these ultramafic and mafic rocks formed with a mantle plume setting at ~616 Ma, which progressed towards early continental rifting within ~50 Ma. Consequently, the Huargualléa Gabbro unit was interpreted by Spikings et al. (2021) [1] to have formed during attenuation of Gondwanan crust, that ultimately lead to the formation of Iapetus oceanic lithosphere by ~550 Ma, and thus it records the initiation of a Wilson cycle that disassembled the continent of Pannotia (e.g., [96,97]; Figure 8A).

A-type plutons in the Eastern Cordillera of Peru ([14]), Precordillera Terrane ([98]) and the Appalachian mountains [99] that formed during 774–691 Ma may reveal an early albeit failed rifting phase along eastern Laurentia within Rodinia. Coeval rocks are not exposed north of Peru, although they were minor source regions for sediments that were ultimately deposited within Carboniferous basins in Ecuador and Colombia (e.g., [1,10]).

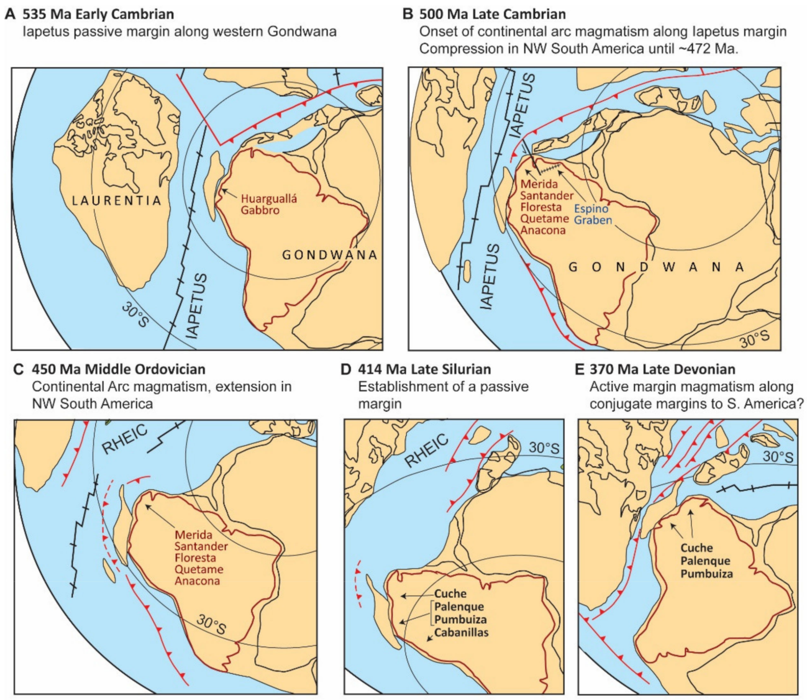

Figure 8. *Cont.*

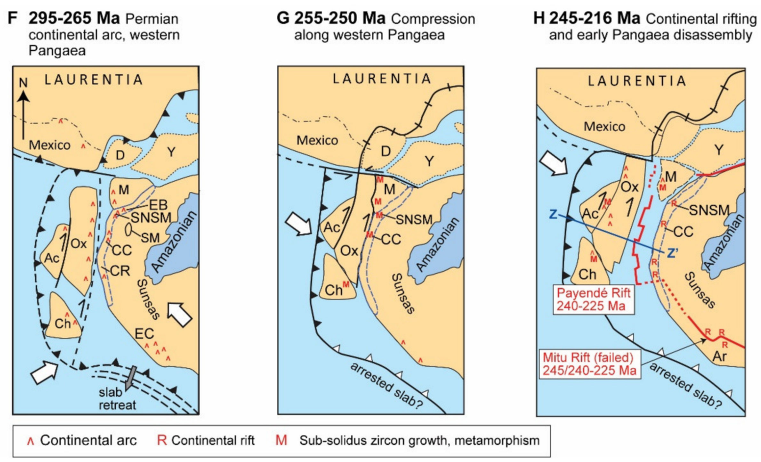

Figure 8. (**A**–**E**) Plate reconstructions for the Palaeozoic margin of northwestern Gondwana, modified and simplified from Cocks and Torsvik (2006) [100] and Van der Lelij et al. (2016) [2]. The location of the Huarguallá Gabbro and other basement sequences are shown, along with the Espino Graben, and some sedimentary formations (labelled in black). (**F**–**H**) Tectonic reconstructions for the Permian and Triassic, modified after Dickinson and Lawton (2001) [101], Elías-Herrera and Ortega-Gutiérrez (2002) [102], Weber et al. (2007) [27], Spikings and Paul (2019) [1], and Spikings et al. (2021) [1].

6.2. Cambrian to Carboniferous

Variably foliated and gneissic granites and granodiorites in the Mérida Andes and Santander Massif crystallised during 499–414 Ma, while similar aged yet more geographically scattered and variably metamorphosed intrusions are found along the western flanks of the Cordillera Central (including the Anacona Block; [8]), the Quetame and Floresta massifs, the Caribbean Mountains of Venezuela, the El Baul Massif and the Llanos Basin. All of these units have geochemical (Figure 5A) and isotopic compositions (Figure 6B,C) that are consistent with continental arc magmatism through Gondwanan crust. The arc rocks are coeval with the Famatinian arc (e.g., [58] and references therein) and arc-related intrusions in the Eastern Cordillera of Peru, and probably represent the northern extent of the same arc-subduction system ([1]; Figure 8B,C). Most of the intrusions that formed during ~499–467 Ma are strongly foliated [2,103] synkinematic granitoids, and intruded during a period of upper amphibolite facies Barrovian metamorphism that affected all rocks older than ~467 Ma. This period is characterised by crustal εHft (zircon) with old Lu-Hf model ages (~1.2–1.7 Ga) and high d^{18}O (quartz; >12‰) values, suggesting a compressive phase occurred between 499–467 Ma ([2]; Figure 9A). Previous authors have related Early Palaeozoic orogenesis in the Northern Andes to the docking of an allochthonous terrane which included the basement of the Santander Massif (Chibcha Terrane; e.g., Ramos, 2009). However, as shown by Van der Lelij et al. (2016) [2], Pb isotopic data collected from granitoids and gneisses from both the Mérida Andes and the Santander Massif (Figure 6B) are consistent with an autochthonous origin, and Nd and Hf isotopic trends (Figure 6A,C) are similar for rocks from the Santander Massif and the Mérida Andes, providing further support for a common history along the margin of Gondwana. Ordovician orogenesis in the Mérida Andes and the Santander Massif was probably driven by increased plate coupling between subducting oceanic lithosphere of the Iapetus Ocean and the overriding margin of Gondwana (e.g., see [104,105]), in a similar setting to Early Palaeozoic orogenic belts elsewhere along the margin of Gondwana (e.g., [106–108]).

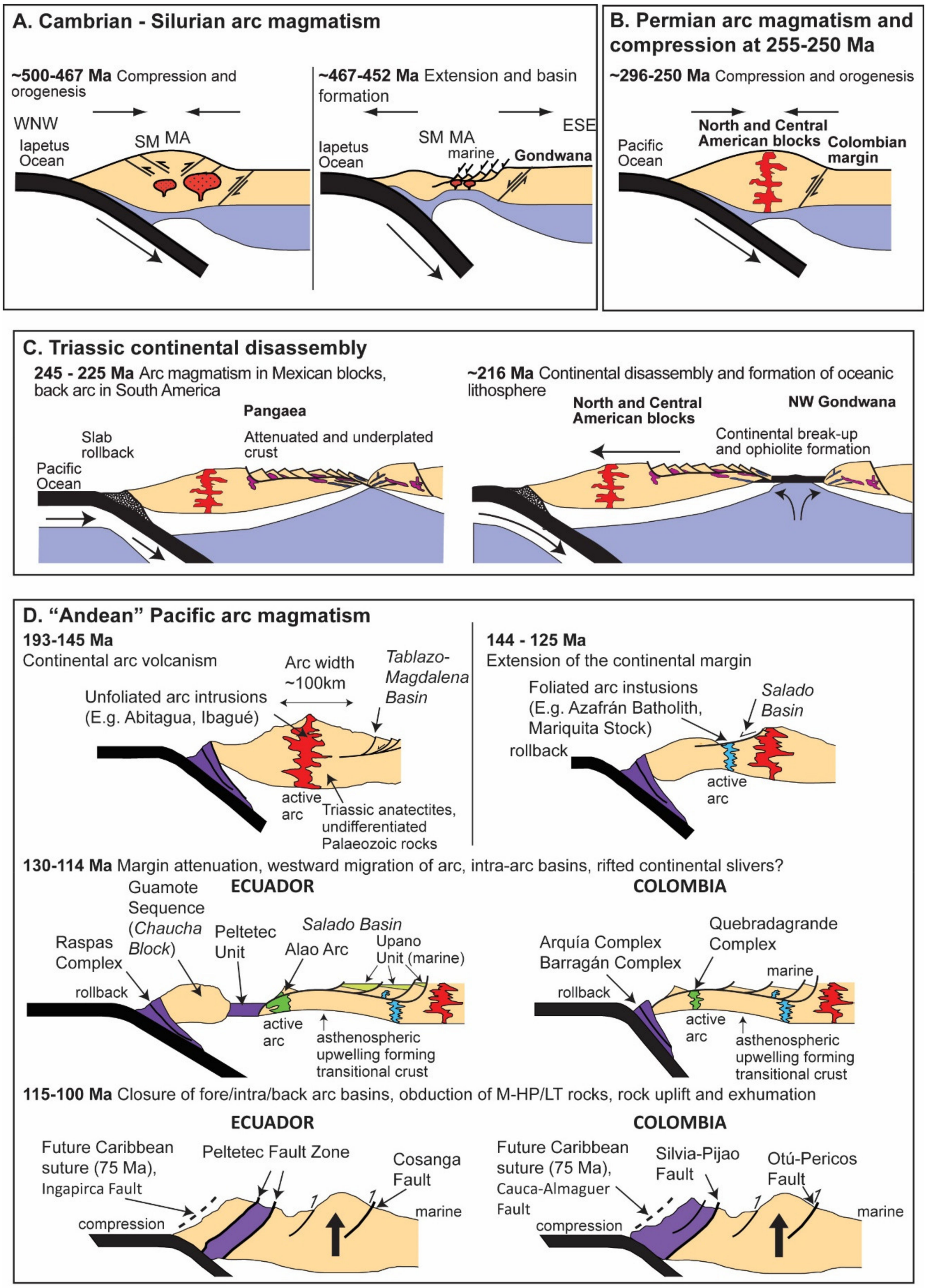

Figure 9. Simplified cross-section models for (**A**) the Cambrian–Earliest Devonian, showing the compressive phase during 499–467 Ma (from [2]), (**B**) Permian continental arc magmatism (296–250 Ma) in a compressive, metamorphic setting during ~255–250 Ma, (**C**) a rift-to-drift transition originating in the Triassic back-arc during 245–216 Ma, giving rise to bimodal magmatism and the formation of oceanic lithosphere (from [24]), (**D**) Prolonged continental arc magmatism forming generally unfoliated high-K calc-alkaline intrusions in the Merida Andes and Santander Massif during 213–194 Ma, a wide (~100 km) unfoliated calc-alkaline arc in the cordilleras Central and Real during 193–145 Ma, and younger foliated arcs during 144–112 Ma that formed on highly attenuated crust. The amount of extension increased southwards, detaching continental crust and forming transitional crust in Ecuador (from [36,43]).

The identification of compression during ~499–467 Ma is significant because it contrasts with older models for the early Rheic Ocean that suggest it opened along northwestern Gondwana during ~505–480 Ma (e.g., [109–112]). Van der Lelij et al. (2016) [2] reconciled apparently simultaneous compression and extension by limiting the extent of the rifted margin such that it did not extend to the region of the rocks of the Mérida Andes and the Santander Massif, and that its westernmost extent is represented by the Palaeozoic Espino Graben ([13]; eastern Venezuela; Figure 1 inset; Figure 8B) where Precambrian and Palaeozoic rocks are truncated by the Caribbean Plate.

The early foliation is crosscut by granitoids that intruded during ~467–414 Ma, and thus these are interpreted to post-date peak metamorphic conditions [2,103]. The upper amphibolite facies metamorphic basement is unconformably overlain by marine sedimentary rocks and tuffs (dated at 453 $\pm$ 3 Ma; [2]) that host volcanogenic massive sulphides (Mucuchachi Fm.), suggesting that marine basins had covered the Cambrian–Early Ordovician metamorphic basement by ~453 Ma [2]. Zircon εHft values span between -4 and +6, corresponding to Lu-Hf model ages of ~0.8–1.3 Ga, and εNdt and quartz $\delta^{18}O$ values range between -6 to +1.5 and 10.30 to 14.27, respectively. These data suggest that the granitoids were derived from a mixture of depleted mantle sources and continental crust, or enriched mantle sources, although these units are clearly derived from a more juvenile source than the preceding metamorphosed basement units. Changes in the degree of deformation, metamorphism and isotopic compositions suggest that the orogen, which included an active continental arc, was subsiding after ~467 Ma (Figure 9A), perhaps as a consequence of either orogenic collapse (e.g., during delamination), or trench retreat that thinned intra-arc or back-arc crust. Tazzo-Rangel et al. (2019) [3] report that most hornblende bearing orthogneisses yield U-Pb ages of ~450 Ma, and interpret these to reflect a phase of compression. This is consistent with Van der Lelij et al. (2016) [2], who interpret an unconformity in the southern Merida Andes (Caparo Block) to be due to a period of compression starting at ~450 Ma.

The lack of Cambrian-Earliest Devonian magmatism in Ecuador is considered by Spikings et al. (2021) [1] to reflect its inboard position due to the presence of outboard arc-crustal blocks (Figure 8B–D) that now form part of southwestern North America. Ordovician magmatism is recorded in the Maya Block (e.g., [113]) and the Acatlán Complex [114], which rifted from Gondwana during 245–216 Ma [115] (Figure 8F–H). Abundant Ordovician magmatism within the Mérida Andes and Santander Massif, along with minor exposures in the Cordillera Central, Quetame and Floresta Massifs of Colombia suggests that these rocks originated within an arc zone located north of the outboard terranes (Figure 8B), which was distal to the Triassic rift. This interpretation is consistent with the lack of Triassic rift-related rocks in these units.

A significant paucity of magmatism in Ecuador, Colombia and Venezuela during ~414 and ~296 Ma, combined with a paucity of Devonian-aged detrital zircons in Carboniferous basins in Ecuador, Peru and farther south suggests this period is not characterised by a continuous ocean-continent subduction system. However, Horton et al. (2010) [10] found a minor peak of Devonian-aged detrital zircons in Devonian sedimentary rocks in Colombia, and Spikings et al. (2021) [1] document Carboniferous detrital zircons in Carboniferous sedimentary units in Ecuador and Colombia. Furthermore, reference [19] report small Carboniferous tonalitic stocks in the northern Cordillera Central of Colombia that formed during 330–310 Ma. Spikings et al. (2021) [1] suggest that the Devonian and a majority of the detrital Carboniferous zircons may be derived from igneous rocks that formed on continental crust that rifted from northwestern South America during the Triassic [24,115] (Figure 8E). These potentially rifted units include a Carboniferous tholeiitic to calc-alkaline arc in the Acatlán Complex [116], continental arc plutons that intrude the microcontinent of Oaxaquia (e.g., [25]), granitic intrusions of the Altos Cuchumatanes (Maya Block) in Guatemala [117], the Aserradero Rhyolite of the Sierra Madre terrane [118], and the La Pezuña Rhyolite of the Coahuila Terrane [119]. Kirsch et al. (2012) [116] and Ortega-

Obregón et al. (2014) [25] suggested these rocks formed within a continental arc setting that commenced at ~330 Ma.

Four Carboniferous $^{40}Ar/^{39}Ar$ white mica plateau dates from Ordovician igneous rocks span between 407–342 Ma [26,83]. Furthermore, Correa-Martinez et al. (2020) [9] suggest that zircon U-Pb ages of magmatic rims of the La Aguadita Amphibolite suggest it was metamorphosed after ~435 Ma. These few dates have been obtained from Ordovician intrusive rocks that are current geographically disparate (western Cordillera Central, Mérida Andes, Santander Massif). The interpretation of all of these dates is ambiguous because laser spot U-Pb zircon and $^{40}Ar/^{39}Ar$ muscovite dates can be mixed ages and thus they may be partially overprinted by late Permian or younger metamorphic events. Despite this, Vinasco et al. (2006) [26] suggested the $^{40}Ar/^{39}Ar$ dates from the Cordillera Central may record retrogression after Carboniferous amphibolite facies metamorphism.

6.3. Permian

Permian granitoids, including mylonitised granites and orthogneisses (Figure 1) exposed in the Sierra Nevada de Santa Marta, the central Cordillera Central, a single location in the far southern Cordillera Real and geographically scattered regions within Venezuela (e.g., El Baul Massif) yield zircon U-Pb dates spanning between 294–253 Ma. The Aluminium Saturation Index of these Permian alkali-calcic to calcic granites straddles the peraluminous and metaluminous fields (Figure 5D), while the $\delta^{18}O$ values (quartz) of 14–17‰ (Figure 6D) suggests that some of these syenogranites formed by partial melting of sedimentary rocks. Zircon Th/U ratios of 0.26–1.27 (see references in [24]) suggest that they crystallised from magmas and have not undergone sub-solidus metamorphic recrystallisation. This is consistent with a high Y content (550–7750 ppm) and negative Eu anomalies in zircons of the El Encanto orthogneiss [11] (Sierra Nevada de Santa Marta). Whole rock trace element abundances are characteristic of subduction related magmatism, which was not bimodal and all rocks yield >58 wt% SiO_2. These variably foliated intrusions have been interpreted to have formed within a continental arc above an east dipping Pacific subduction zone beneath western Pangaea [7,11,20,21,24] during 294–253 Ma (Figures 8F and 9B).

Inherited Early Neoproterozoic and Ordovician zircon cores are common in Permian intrusions in Colombia and Ecuador (see references in [24]), and thus the Permian continental arc recycled Sunsas and Famatinian-aged crust, which is consistent with the mildly peraluminous and calc-alkaline compositions. Cathodoluminescence images show that many detrital zircons from the Gaira Schists (Sierra Nevada de Santa Marta) consist of Ordovician cores [11] with Permian rims, which suggests that Permian magmas recycled the older Ordovician arc sequence. These are consistent with the model Lu-Hf ages (0.65–1.2 Ga; Figure 6C) of most of the Permian intrusions, which overlap with the model ages obtained from the Cambrian–Earliest Devonian intrusions. The uncorrected Pb isotopic compositions of the Cambrian–Earliest Devonian and Permian intrusions are also similar, suggesting they formed on the same Gondwanan crust.

The Permian intrusions within the Sierra de Perijá, Paraguaná Peninsula and the El Baúl Massif within Venezuela are currently located up to ~500 km to the east of the Sierra Nevada de Santa Marta and the Cordillera Central (Figure 1), whereas there is a magmatic gap between 414–294 Ma in the Santander Massif [2], which is only located 200–150 km east of the Cordillera Central (Figure 1). Spikings and Paul (2019) [24] suggested that the El Baúl Massif may have been closer to the continental margin before north-eastward movement of the Maracaibo Block during the Cenozoic [120], and the rocks of the Santander Massif were located east of the Permian arc axis (Figure 8F).

Regional metamorphism at the end of the Permian is recorded in South America by prograde metamorphism in the Sierra Nevada de Santa Marta to ~770–830 °C and ~11.5–14 kb (hbl-grt; hbl-plag-qtz), followed by retrogression to 530 °C and 5.5 kb, with sub-solidus metamorphic zircon cores that were coeval with garnet growth at ~250 Ma [11]. Kinked plagioclase in mylonitic Permian intrusions (288–264 Ma) of the Sierra Nevada de Santa Marta, were interpreted by Cardona et al. (2010) [20] as a high temperature (>450 °C) deformation event. The same authors interpret amphibole K-Ar dates of ~250 Ma [121] from a gneissic clast located proximal to the mylonites to be the result of a thermal disturbance at ~250 Ma, which was responsible for the high-temperature deformation of the Permian intrusions. Finally, the Th/U content of late Permian zircons at ~255–250 Ma approaches 0.1, corroborating sub-solidus zircon growth and a metamorphic event at that time [24].

MP-HT metamorphism has also been recorded in the Triassic conjugate margins, for example low Th/U ratios <0.1 in zircons from migmatites of the Chiapas Massif and the Chortis Block during 255–250 Ma [27,28]. Weber et al. (2007) [27], Cardona et al. (2010) [20] and Spikings and Paul (2019) [24] attribute metamorphism in the Chiapas Massif and northwestern South America to compression that closed marginal basins during the waning stages of the amalgamation of Pangaea. The collision event post-dates the early amalgamation of Pangaea by ~50 Ma, which is recorded along the diachronous Ouachita-Marathon suture that had formed by the Early Permian. This compressive period is consistent with rapid cooling of an Ordovician granite in the Mérida Andes during ~260–250 Ma [83], via accelerated rock uplift and exhumation. Model Lu-Hf ages in 255–250 Ma intrusions are older than 1 Ga (Figure 6C), implying that crustal thickening may have placed rocks with longer crustal residence times into the collision zone.

6.4. Triassic

Triassic crustal anatectites of the Sierra Nevada de Santa Marta and Cordillera Central of Colombia, and the Amotape Complex and Cordillera Real of Ecuador that formed during 250–208 Ma are highly peraluminous with high $d^{18}O$ (quartz, >12; Figure 6E), and εHf_t as low as -13 (Figure 6C), suggesting that pelitic rocks melted after ~250 Ma. Extremely low Th/U values (<0.1) in some Triassic zircon rims suggest some Triassic igneous zircons re-crystallised during the Triassic during high-T metamorphism (Spikings and Paul, 2019). This period was also characterised by bimodal magmatism, with amphibolitised basaltic dykes and sills during ~243–216 Ma.

The compositions of the mafic, tholeiitic dykes are consistent with a back-arc basin or MORB setting (Figure 5C,E,F), and the progressive trend in isotopic compositions towards the depleted mantle (Figure 6A–C) suggests they were emplaced within a lithosphere that was thinning. εHf_i (zircons) show that mantle derived tholeiites emplaced during 243–232 Ma assimilated isotopically evolved continental crust (Figure 6C), whereas there is little evidence of the assimilation of significant crust after 225 Ma, when εHf_i approaches depleted mantle compositions. Pb isotopes in feldspars (Figure 6B) also reveal mixing between a highly radiogenic component that is compatible with upper continental crust, with a juvenile source that approaches the depleted mantle and is represented by the mafic end member rocks.

The widespread occurrence of coeval tholeiitic, basaltic dykes and crustal anatectites within Colombia and Ecuador (Figure 1) supports an extensional setting, which has been interpreted as a back-arc (e.g., [24,122]; Figure 8H). The arc units are preserved in the conjugate margins of the Chaucús Complex (Guatemala), the Chortis Block (Ovejas Complex, inheritance in Eocene intrusions), the Rabinal Complex (Maya Block), and the Ayú Complex (granitic dykes; Mixteca Terrane; see references in [24]). Rifting within northwestern South America during 250–216 Ma represents the early disassembly of western Pangaea (Figure 8H) [21,36,115]. Mafic underplating and crustal anatexis was a result of decompression of the asthenosphere during passive extension, and heat convection via the mafic magmas into the crust (Figure 9C). Spikings and Paul (2019) [24] refer to this rift as the Payendé Rift (Figure 8H), which was also used by Senff (1995) [123] and Cediel and Cáceres (2000) [124] to describe the tectonic setting of Triassic, red siliclastic rocks of the Payendé Fm. in northern Colombia. Correa-Martínez (2007) [38] documents a series of metagabbros, amphibolites and plagiogranites from the northern Cordillera Central, and concludes that they are part of an ophiolitic sequence (the Aburrá Ophiolite) that formed within a back-arc basin. U-Pb dating of magmatic zircons from a plagiogranite yields an age of ~216 Ma suggesting that seafloor spreading started between ~225 and ~216 Ma (Figure 9C).

6.5. Latest Triassic–Early Cretaceous (213–112 Ma)

Magmatism along northwestern South America commenced at ~213 Ma, and its unimodal (with respect to SiO_2), metaluminous, high-K to calc-alkaline character contrasts with Triassic magmatism, and marks the formation of a new subduction zone inboard of the Triassic Central and North American terranes. Arc magmatism during 213–194 Ma was focused within the rocks of the Santander Massif [2,5], currently located 280–350 km inboard of the Silvia-Pijao Fault, while fewer intrusions are found in the Mérida Andes (Figure 1) [2]. These early arc magmas are highly enriched in LILE (Figure 5B), LREE and non-radiogenic Nd and Hf isotopes (Figure 6A,C), and mainly formed by melting regions that had formed part of the continental crust for at least 1 Ga.

The arc axis migrated generally slowly westwards after ~194 Ma, opening continental and shallow marine depocenters (Cediel, 2018). The overall westward shift formed a long-lived calc-alkaline, metaluminous arc (193–145 Ma; red colours in Figures 1 and 9D) which is defined by several batholiths in the Cordillera Central and Cordillera Real (e.g., [6,41,43,44,46]). Jurassic plutons are also exposed along the western and eastern flanks of the Upper Magdalena Valley in southern Colombia [42] (Figure 1), and there are several Jurassic volcanic formations (e.g., the Misahuallí Fm. in Ecuador). This younger belt yields significantly more radiogenic Nd (Figure 6A) and Hf (Figure 6C) isotopic compositions, and the rocks are less enriched (Figure 5A) and more metaluminous (Figure 5B) than during 213–194 Ma, suggesting they are either derived from a more juvenile source or have assimilated less continental crust. A comparison of age and longitude suggests that magmatism during 193–145 Ma was focussed in a zone with a width of ~100km (Figures 4 and 9d), while the oldest intrusions occur along the eastern flanks of the Cordillera Central (e.g., San Lucas Batholith; Figure 1). Spikings et al. (2019) [43] suggested that the progressive increase in radiogenic Hf and Nd isotopic compositions during 213–145 Ma, combined with a steady trend from high-K calc-alkaline to calc-alkaline compositions indicates that arc magmatism progressively assimilated a smaller proportion of evolved continental crust during 213–145 Ma. The same authors hypothesised that the crust was generally thinning throughout 213–145 Ma during low rates of extension, creating an arc with significant arc width (~100km), and that extension may have been driven by slab retreat (Figure 9D). The trench-arc distance at various latitudes oscillated during 193–145 Ma (e.g., [6,41,44]) due to short temporal variations in slab dip that typically span ~10 Myr (e.g., [125]), although the geochemical and isotopic data provides a compelling argument for a prevailing albeit punctuated extensional regime.

The metaluminous continental arc continued after 145 Ma, although unlike the period during 213–145 Ma, the intrusions that formed during 144–125 Ma (Azafrán and Chinguál Batholiths, and the Mariquita Stock) are pervasively foliated (e.g., [126]). Regardless, these younger intrusions are consistent with the older trend towards more juvenile Hf and Nd compositions (Figure 6A,C). The combination of pervasive foliation and juvenile isotopic compositions lead Spikings et al. (2015, 2019) [36,43] to suggest they erupted through thinned crust in an active extensional system (Figure 9D), and that extensional rates increased at ~144 Ma. Extension during 144–125 Ma coincides with (i) high sedimentation rates in Early Cretaceous rifts located along the eastern flank of the Eastern Cordillera [127–129], and (ii) extension of the basement of the Oriente Basin in Ecuador [88] and in northern Peru [89]. Increased cooling rates of the Ibagué Batholith south of the Ibagué Fault (Figure 7A) are interpreted to be related to exhumation of the intrusion during extension.

Younger mafic, calk-alkaline to tholeiitic volcanic continental arc rocks of the Alao and Quebradagrande Complexes (~118–112 Ma; see Section 3.7) are preserved to the west of the Azafrán and Chinguál Batholiths, and west of an uplifted basement core [126] of Palaeozoic basement and Triassic migmatites (green colours in Figures 1 and 9D). The volcanic rocks also continue the trend towards more juvenile Nd and Hf isotopic compositions (Figure 6A,C), and they are more depleted in trace elements relative to the older arc intrusions (Figure 5B). Furthermore, Pb isotopic compositions suggest the arc units during 213–112 Ma assimilated the same Gondwanan crust (Figure 6B), which corroborates the presence of large volumes of quartz-zircon-tourmaline rich arenites [36,46] supporting an interpretation that these are continental arcs.

The Alao and Quebradagrande arcs were interpreted [7,36,43,46,64] to have formed above an east-dipping subduction zone along the thinned fringe of a continental margin. Paul et al. (2018) [23] and Spikings et al. (2019) [43] suggest that the amount of extension increased towards the south, and was greatest within Ecuador (Figure 9D). This interpretation is consistent with (i) the generation of depleted mantle melts that formed E-MORB rocks of the Peltetec Unit at ~135 Ma in Ecuador [36], which have not been identified in Colombia, (ii) rifting and the detachment of Jurassic continental crust of the Chaucha Block (Figure 1) in Ecuador, and (iii) Early Cretaceous re-heating of the Triassic crystalline units in Ecuador to T > 380 °C, which did not occur in Colombia (Figure 7A).

The simplest explanation for the geochemical, isotopic and geochronological trends obtained from the Jurassic and Early Cretaceous igneous rocks is that they formed above the same east-dipping subduction zone that started at ~213 Ma, and which was generally retreating oceanward after ~194 Ma, and after ~145 Ma until ~112 Ma (e.g., [36]; Figure 9D).

7. Conclusions

Overall, a combination of accurate estimates of the time of crystallisation of igneous rocks and subsequent metamorphism, geochemical constraints on magmatic processes, isotopic constraints on magma source regions and continuous thermal history information clearly identify periods of rifting, passive and active margins and continent amalgamation, which record a transition from the Iapetus to Pacific Wilson cycles in northwestern South America.

1. Rifting and the initiation of the Wilson Cycle during 623–531 Ma is recorded by olivine bearing gabbros and ultramafic rocks of the Huargualláá Gabbro unit that is exposed along the western flank of the Cordillera Real, and a nepheline syenite in the Llanos Basin of Colombia. The units form part of the geographically dispersed Central Iapetus Magmatic Province, and their location is consistent with the continental reconstruction of Tegner et al. (2019) [95], which juxtaposes northwestern Gondwana with late Neoproterozoic dyke complexes within Baltica. Stratigraphic constraints on the formation of rift-basalts of the Puncoviscana Belt (Argentina), suggests they formed within the same setting, during the rift stage of the Iapetus Wilson Cycle.
2. Subduction of Iapetan oceanic lithosphere gave rise to active margin magmatism in northwestern Gondwana during ~499 Ma ~414 Ma, The period during 499–467 is characterised by compression, forming orthogneisses with a pervasive foliation and upper amphibolite Barrovian metamorphism. Compression was coeval with extension located further east along the northern Gondwanan margin, during the opening of the Rheic Ocean, suggesting that Iapetan oceanic lithosphere was being subducted to the west of the Rheic rift axis. Extension prevailed after ~467 Ma, possibly due to westward propagation of the Rheic extensional axis, and perhaps also as a response to gravitational collapses of the orogen, although this is not constrained. These intrusions are mainly preserved inboard of younger arcs (Mérida Andes and the Santander Massif), although smaller Ordovician crustal blocks are preserved in the Cordillera Central, which may be windows to an extensive Ordovician basement sequence. The arc rocks are coeval with the Famatinian arc and arc-related intrusions in the Eastern Cordillera of Peru, and probably represent the northern extent of the same arc-subduction system. The occurrence of hornblende orthogneisses and an unconformity in the southern Merida Andes during 453–445 Ma may be a consequence of a second compressive phase that started at ~450 Ma. The isotopic compositions of the Cambrian–Earliest Devonian intrusions suggest they share a common history

along the margin of Gondwana, and are not derived from Laurentia. The lack of Cambrian-Earliest Devonian magmatism in Ecuador reflects its inboard position relative to arc-crustal blocks that now form part of southwestern North America, and detached during Triassic rifting.

3. With the exception of minor Carboniferous stocks that formed during 330–310 Ma, the period during ~414 and ~296 Ma is characterised by a paucity of magmatism. The origin of a minor peak of Devonian-aged detrital zircons in Devonian sedimentary rocks in Colombia remains enigmatic, and Carboniferous detrital zircons in Carboniferous sedimentary units may be derived from an arc on the Triassic rifted conjugate margin, or from the south (e.g., Peru). Carboniferous $^{40}Ar/^{39}Ar$ white mica plateau dates (407–342 Ma) and some zircon U-Pb ages of magmatic rims of geographically dispersed Ordovician igneous rocks have been interpreted to record a possible Carboniferous period of amphibolite facies metamorphism, which may reflect collision events between Laurentia and Gondwana, during the early stages of the amalgamation of Pangaea.
4. Subduction of Pacific lithosphere formed a continental arc during 294–253 Ma along western Pangaea, which was dismembered in South America by sinistral displacement along the southern Caribbean Plate boundary Zone, and is preserved in geographically dispersed regions. The arc reworked and assimilated Sunsas (~1 Ga) and Famatinian (Cambrian-Earliest Devonian) continental crust. Compression drove regional metamorphism, rock uplift and exhumation at the end of the Permian (255–250 Ma), which is recorded in the Mérida Andes, Sierra Nevada de Santa Marta, and the Triassic conjugate margins including the Chiapas Massif and the Chortis Block, forming the waning stage of the amalgamation of Pangaea ~50 Ma after the Ouachita-Marathon suture.
5. Magmatic underplating and anatexis of continental crust during 245–225 Ma occurred during progressive thinning of the continental lithosphere during rifting along western Pangaea. Rifting advanced to complete separation of continental crust by ~216 Ma, and the formation of oceanic lithosphere between the conjugate margins of northwestern South America and basement terranes of Mexico and Central America. The rifting event is recorded by amphibolitised tholeiitic basaltic dykes and extensive tracts of migmatites and S-type granites within the conjugate margins. Various Triassic units in the Chaucús Complex, Chortis Block, Maya Block, the Mixteca Terrane (Mexico and Central America) formed within the Triassic arc and back-arc. Rifting north of the Huancabamba Deflection was accompanied by subduction, and occurred within a backarc. Triassic rifting represents the early stage of the fragmentation of Pangaea, eventually leading to the opening of the proto-Caribbean Seaway and Central Atlantic at ~195 Ma.
6. East-dipping subduction of the Farallon Plate formed a calc-alkaline continental arc that commenced in northwestern South America at ~213 Ma, representing the onset of the Andean cycle. The arc axis migrated oceanward at ~194 Ma, and formed a long/lived continental arc during 193–112 Ma within Colombia and Ecuador, and was accompanied by progressive thinning of the continental crust. Trench retreat of the east dipping-subduction zone accelerated along northwestern South America at ~144 Ma, and extension during 144–115 Ma formed syn-tectonic granitoid intrusions within Ecuador, attenuated the continental margin forming thin intra-arc basins characterised by transitional crust, and resulted in an oceanward migration of the arc axes, which became progressively more isotopically juvenile and geochemically depleted. Rapid extension rifted some narrow continental slivers (e.g., the Chaucha Block) from the margin.

Author Contributions: Conceptualization, R.S.; investigation, R.S., R.V.d.L.; data curation, R.S., R.V.d.L.; writing—original draft preparation, R.S.; writing—review and editing, R.S.; supervision, R.S.; project administration, R.S.; funding acquisition, R.S. All authors have read and agreed to the published version of the manuscript.

Funding: This research was funded by Swiss National Science Foundation grants 200020_134443 and 200020_146332, which were awarded to R.S.

Data Availability Statement: This is a review, and therefore all data can be found indexed from the original sources in the citations that are provided.

Acknowledgments: We thank Cristian Vallejo, Bernado Beate, Arturo Egüez, Etienne Jaillard, Alfredo Buitron, Byron Pelicita and Luis Lopez for assistance in the field in the cordilleras of Ecuador, and Ecopetrol S.A., Andres Mora, Andreas Kammer, Luis Carlos Mantilla, Alejandro Beltran, Jaime Corredor, Jaime Castellanos, Wilson Casallas, and Luis Quiroz for their assistance during field work in Colombia.

Conflicts of Interest: The authors declare no conflict of interest.

References

1. Spikings, R.; Paul, A.; Vallejo, C.; Reyes, P. Constraints on the Ages of the Crystalline Basement and Palaeozoic Cover Exposed in the Cordillera Real, Ecuador: 40Ar/39Ar Analyses and Detrital Zircon U/Pb Geochronology. *Gondwana Res.* **2021**, *90*, 77–101. [CrossRef]
2. Van der Lelij, R.; Spikings, R.; Ulianov, A.; Chiaradia, M.; Mora, A. Palaeozoic to Early Jurassic History of the Northwestern Corner of Gondwana, and Implications for the Evolution of the Iapetus, Rheic and Pacific Oceans. *Gondwana Res.* **2016**, *31*, 271–294. [CrossRef]
3. Tazzo-Rangel, M.D.; Weber, B.; González-Guzmán, R.; Valencia, V.A.; Frei, D.; Schaaf, P.; Solari, L.A. Multiple Metamorphic Events in the Palaeozoic Mérida Andes Basement, Venezuela: Insights from U–Pb Geochronology and Hf–Nd Isotope Systematics. *Int. Geol. Rev.* **2019**, *61*, 1557–1593. [CrossRef]
4. Mantilla Figueroa, L.C.; Bissig, T.; Cottle, J.M.; Hart, C.J.R. Remains of Early Ordovician Mantle-Derived Magmatism in the Santander Massif (Colombian Eastern Cordillera). *J. S. Am. Earth Sci.* **2012**, *38*, 1–12. [CrossRef]
5. Mantilla Figueroa, L.C.; Bissig, T.; Valencia, V.; Hart, C.J.R. The Magmatic History of the Vetas-California Mining District, Santander Massif, Eastern Cordillera, Colombia. *J. S. Am. Earth Sci.* **2013**, *45*, 235–249. [CrossRef]
6. Leal-Mejía, H.; Shaw, R.P.; Melgarejo i Draper, J.C. Spatial-temporal migration of granitoid magmatism and the phanerozoic tectono-magmatic evolution of the Colombian Andes. In *Geology and Tectonics of Northwestern South America*; Frontiers in Earth Sciences; Cediel, F., Shaw, R.P., Eds.; Springer International Publishing: Cham, Germany, 2019; pp. 253–410, ISBN 978-3-319-76131-2.
7. Villagómez, D.; Spikings, R.; Magna, T.; Kammer, A.; Winkler, W.; Beltrán, A. Geochronology, Geochemistry and Tectonic Evolution of the Western and Central Cordilleras of Colombia. *Lithos* **2011**, *125*, 875–896. [CrossRef]
8. Martens, U.; Restrepo, J.J.; Ordóñez-Carmona, O.; Correa-Martínez, A.M. The Tahamí and Anacona Terranes of the Colombian Andes: Missing Links between the South American and Mexican Gondwana Margins. *J. Geol.* **2014**, *122*, 507–530. [CrossRef]
9. Correa-Martínez, A.M.; Martens, U.; Rodríguez, G. Collage of Tectonic Slivers Abutting the Eastern Romeral Fault System in Central Colombia. *J. S. Am. Earth Sci.* **2020**, *104*, 102794. [CrossRef]
10. Horton, B.K.; Saylor, J.E.; Nie, J.; Mora, A.; Parra, M.; Reyes-Harker, A.; Stockli, D.F. Linking Sedimentation in the Northern Andes to Basement Configuration, Mesozoic Extension, and Cenozoic Shortening: Evidence from Detrital Zircon U-Pb Ages, Eastern Cordillera, Colombia. *Geol. Soc. Am. Bull.* **2010**, *122*, 1423–1442. [CrossRef]
11. Piraquive, A.; Kammer, A.; Bernet, M.; Cramer, T.; von Quadt, A.; Gómez, C. Neoproterozoic to Jurassic Tectono-Metamorphic Events in the Sierra Nevada de Santa Marta Massif, Colombia: Insights from Zircon U-Pb Geochronology and Trace Element Geochemistry. *Int. Geol. Rev.* **2021**, 1–33. [CrossRef]
12. Viscarret, P.; Wright, J.; Urbani, F. New U-Pb Zircon Ages of El Baúl Massif, Cojedes State, Venezuela. *Rev. Téc. Ing. Univ. Zulia.* **2009**, *32*, 210–221.
13. Feo-Codecido, G.; Smith, F.D., Jr.; Aboud, N.; di Giacomo, E. Basement and Paleozoic Rocks of the Venezuelan Llanos Basins. *Mem. Geol. Soc.* **1984**, *162*, 173–187.
14. Mišković, A.; Spikings, R.A.; Chew, D.M.; Košler, J.; Ulianov, A.; Schaltegger, U. Tectonomagmatic Evolution of Western Amazonia: Geochemical Characterization and Zircon U-Pb Geochronologic Constraints from the Peruvian Eastern Cordilleran Granitoids. *Geol. Soc. Am. Bull.* **2009**, *121*, 1298–1324. [CrossRef]
15. Restrepo, J.J.; Toussaint, J.F. *Unidades Litologicas de Los Alrededores de Medellın*; Centro Journal: New York, NY, USA, 1984; pp. 1–26.
16. Bustamante, A.; Juliani, C. Unraveling an Antique Subduction Process from Metamorphic Basement around Medellín City, Central Cordillera of Colombian Andes. *J. S. Am. Earth Sci.* **2011**, *32*, 210–221. [CrossRef]
17. Litherland, M.; Aspden, J.A.; Jemielita, R.A. *The Metamorphic Belts of Ecuador*; Overseas Memoir of the British Geological Survey; British Geological Survey: Nottingham, UK, 1994; Volume 11.
18. Gomez, J.; Nivia, A.; Jimenez, D.M.; Tejada, M.L.; Sepulveda, J.; Osorio, J.A.; Gaona, T.; Dieferix, H.; Uribe, H.; Mora, M. Geological Map of Colombia 2007. Escala 1:1′000.000. Available online: https://www2.sgc.gov.co/ProgramasDeInvestigacion/Geociencias/Documents/Descargables/Gomez-et-al-2007_GMC_PDF.pdf (accessed on 10 November 2021).

19. Leal-Mejia, H.; Draper, J.; Shaw, R. Phanerozoic gold metallogeny in the Colombian Andes. In Proceedings of the Let's Talk Ore Deposits—Eleventh Biennial SGA Meeting, Antofagasta, Chile, 26–29 September 2011.
20. Cardona, A.; Valencia, V.; Garzón, A.; Montes, C.; Ojeda, G.; Ruiz, J.; Weber, M. Permian to Triassic I to S-Type Magmatic Switch in the Northeast Sierra Nevada de Santa Marta and Adjacent Regions, Colombian Caribbean: Tectonic Setting and Implications within Pangea Paleogeography. *J. S. Am. Earth Sci.* **2010**, *29*, 772–783. [CrossRef]
21. Cochrane, R.; Spikings, R.; Gerdes, A.; Ulianov, A.; Mora, A.; Villagómez, D.; Putlitz, B.; Chiaradia, M. Permo-Triassic Anatexis, Continental Rifting and the Disassembly of Western Pangaea. *Lithos* **2014**, *190–191*, 383–402. [CrossRef]
22. Bustamante, C.; Archanjo, C.J.; Cardona, A.; Bustamante, A.; Valencia, V.A. U-Pb Ages and Hf Isotopes in Zircons from Parautochthonous Mesozoic Terranes in the Western Margin of Pangea: Implications for the Terrane Configurations in the North Andes. *J. Geol.* **2017**, *125*, 487–500. [CrossRef]
23. Paul, A.N.; Spikings, R.A.; Ulianov, A.; Ovtcharova, M. High Temperature (>350 °C) Thermal Histories of the Long Lived (>500 Ma) Active Margin of Ecuador and Colombia: Apatite, Titanite and Rutile U-Pb Thermochronology. *Geochim. Cosmochim. Acta* **2018**, *228*, 275–300. [CrossRef]
24. Spikings, R.A.; Paul, A. *The Permian—Triassic History of Magmatic Rocks of the Northern Andes (Colombia and Ecuador): Super-continent Assembly and Disassembly*; Servicio Geológico Colombiano: Bogotá, Columbia, 2019; p. 15.
25. Ortega-Obregón, C.; Solari, L.; Gómez-Tuena, A.; Elías-Herrera, M.; Ortega-Gutiérrez, F.; Macías-Romo, C. Permian–Carboniferous Arc Magmatism in Southern Mexico: U–Pb Dating, Trace Element and Hf Isotopic Evidence on Zircons of Ear-liest Subduction beneath the Western Margin of Gondwana. *Int. J. Earth Sci.* **2014**, *103*, 1287–1300. [CrossRef]
26. Vinasco, C.J.; Cordani, U.G.; González, H.; Weber, M.; Pelaez, C. Geochronological, Isotopic, and Geochemical Data from Permo-Triassic Granitic Gneisses and Granitoids of the Colombian Central Andes. *J. S. Am. Earth Sci.* **2006**, *21*, 355–371. [CrossRef]
27. Weber, B.; Iriondo, A.; Premo, W.R.; Hecht, L.; Schaaf, P. New Insights into the History and Origin of the Southern Maya Block, SE México: U–Pb–SHRIMP Zircon Geochronology from Metamorphic Rocks of the Chiapas Massif. *Int. J. Earth Sci.* **2007**, *96*, 253–269. [CrossRef]
28. Ratschbacher, L.; Franz, L.; Min, M.; Bachmann, R.; Martens, U.; Stanek, K.; Stübner, K.; Nelson, B.K.; Herrmann, U.; Weber, B.; et al. The North American-Caribbean Plate Boundary in Mexico-Guatemala-Honduras. *Geol. Soc. Lond. Spec. Publ.* **2009**, *328*, 219–293. [CrossRef]
29. Ward, D.E.; Goldsmith, R.; Restrepo, H.A. Open-File Report. 1974. Available online: https://pubs.er.usgs.gov/publication/ofr74258 (accessed on 10 November 2021).
30. Montes, C.; Guzman, G.; Bayona, G.; Cardona, A.; Valencia, V.; Jaramillo, C. Clockwise Rotation of the Santa Marta Massif and Simultaneous Paleogene to Neogene Deformation of the Plato-San Jorge and Cesar-Ranchería Basins. *J. S. Am. Earth Sci.* **2010**, *29*, 832–848. [CrossRef]
31. Weber, M.; Cardona, A.; Valencia, V.; García-Casco, A.; Tobón, M.; Zapata, S. U/Pb Detrital Zircon Provenance from Late Cretaceous Metamorphic Units of the Guajira Peninsula, Colombia: Tectonic Implications on the Collision between the Car-ibbean Arc and the South American Margin. *J. S. Am. Earth Sci.* **2010**, *29*, 805–816. [CrossRef]
32. Restrepo, J.J.; Ordóñez-Carmona, O.; Armstrong, R.; Pimentel, M.M. Triassic Metamorphism in the Northern Part of the Tahamí Terrane of the Central Cordillera of Colombia. *J. S. Am. Earth Sci.* **2011**, *32*, 497–507. [CrossRef]
33. Aspden, J.A.; McCourt, W.J.; Brook, M. Geometrical Control of Subduction-Related Magmatism: The Mesozoic and Cenozoic Plutonic History of Western Colombia. *J. Geol. Soc.* **1987**, *144*, 893–905. [CrossRef]
34. Chew, D.; Magna, T.; Kirkland, C.; Miskovic, A.; Cardona, A.; Spikings, R.; Schaltegger, U. Detrital Zircon Fingerprint of the Proto-Andes: Evidence for a Neoproterozoic Active Margin? *Precambrian Res.* **2008**, *167*, 186–200. [CrossRef]
35. Riel, N.; Guillot, S.; Jaillard, E.; Martelat, J.-E.; Paquette, J.-L.; Schwartz, S.; Goncalves, P.; Duclaux, G.; Thebaud, N.; Lanari, P.; et al. Metamorphic and Geochronogical Study of the Triassic El Oro Metamorphic Complex, Ecuador: Implications for High-Temperature Metamorphism in a Forearc Zone. *Lithos* **2013**, *156–159*, 41–68. [CrossRef]
36. Spikings, R.; Cochrane, R.; Villagomez, D.; Van der Lelij, R.; Vallejo, C.; Winkler, W.; Beate, B. The Geological History of Northwestern South America: From Pangaea to the Early Collision of the Caribbean Large Igneous Province (290–75 Ma). *Gondwana Res.* **2015**, *27*, 95–139. [CrossRef]
37. Noble, S.R.; Aspden, J.A.; Jemielita, R. Northern Andean Crustal Evolution: New U-Pb Geochronological Constraints from Ecuador. *Geol. Soc. Am. Bull.* **1997**, *109*, 789–798. [CrossRef]
38. Correa-Martinez, A.M. *Petrogênese e Evolução Do Ofiolito de Aburrá, Cordilhera Central Dos Andes Colombianos*; Universidade de Brasília: Brasilia, Brazil, 2007.
39. Chiaradia, M.; Vallance, J.; Fontboté, L.; Stein, H.; Schaltegger, U.; Coder, J.; Richards, J.; Villeneuve, M.; Gendall, I. U–Pb, Re–Os, and 40Ar/39Ar Geochronology of the Nambija Au-Skarn and Pangui Porphyry Cu Deposits, Ecuador: Implications for the Jurassic Metallogenic Belt of the Northern Andes. *Min. Depos.* **2009**, *44*, 371–387. [CrossRef]
40. Bustamante, C.; Cardona, A.; Bayona, G.; Mora, A.; Valencia, V.; Gehrels, G.; Vervoort, J. U-Pb LA-ICP-MS Geochronology and Regional Correlation of Middle Jurassic Instrusive Rocks from the Garzon Massif, Upper Magdalena Vallez and Central Cor-dillera, Southern Colombia. *Boletín Geol.* **2010**, *32*, 93–109.
41. Bustamante, C.; Archanjo, C.J.; Cardona, A.; Vervoort, J.D. Late Jurassic to Early Cretaceous Plutonism in the Colombian Andes: A Record of Long-Term Arc Maturity. *Geol. Soc. Am. Bull.* **2016**, *128*, 1762–1779. [CrossRef]

42. Rodríguez, G.; Arango, M.I.; Zapata, G.; Bermúdez, J.G. Petrotectonic Characteristics, Geochemistry, and U-Pb Geochronology of Jurassic Plutons in the Upper Magdalena Valley-Colombia: Implications on the Evolution of Magmatic Arcs in the NW Andes. *J. S. Am. Earth Sci.* **2018**, *81*, 10–30. [CrossRef]
43. Spikings, R.A.; Cochrane, R.; Vallejo, C.; Villagomez, D.; Van der Lelij, R.; Paul, A.; Winkler, W. Latest triassic to early cre-taceous tectonics of the Northern Andes: Geochronology, geochemistry, isotopic tracing, and thermochronology. In *Andean Tectonics*; Elsevier: Amsterdam, The Netherlands, 2019; pp. 173–208, ISBN 978-0-12-816009-1.
44. Restrepo, M.; Bustamante, C.; Cardona, A.; Beltrán-Triviño, A.; Bustamante, A.; Chavarría, L.; Valencia, V.A. Tectonic Im-plications of the Jurassic Magmatism and the Metamorphic Record at the Southern Colombian Andes. *J. S. Am. Earth Sci.* **2021**, *111*, 103439. [CrossRef]
45. Colmenares, F. *Evolución Geohistorica de La Sierra Nevada de Santa Marta*; Ingeominas: Bogotá, Colombia, 2007.
46. Cochrane, R.; Spikings, R.; Gerdes, A.; Winkler, W.; Ulianov, A.; Mora, A.; Chiaradia, M. Distinguishing between In-Situ and Accretionary Growth of Continents along Active Margins. *Lithos* **2014**, *202–203*, 382–394. [CrossRef]
47. Bass, M.; Shagam, R. *Edades Rb–Sr de Las Rocas Cristalinas de Los Andes Merideños, Venezuela*; Ministerio de Minas e Hi-drocarburos de Venezuela: Caracas, Venezuela, 1959.
48. Martin-Bellizia, C.; Ramirez, C.; Menendez, A.; Rios, J.H.; Benaim, N. Edades Isotópicas de Rocas Venezolanas. *Boletín Geol.* **1968**, *10*, 356–380.
49. Goldsmith, R.; Marvin, R.F.; Mehnert, H.H. *Radiometric Ages in the Santander Massif, Eastern Cordillera, Colombian Andes*; United States Geological Survey Professional Paper 750-D; United States Geological Survey: Reston, VA, USA, 1971; pp. 44–49.
50. Feininger, T.; Barrero, D.; Castro, N. Geología de Antioquia et Caldas—Sub-Zona II-B. *Bol. Geol. Bogota* **1972**, *20*, 173.
51. Bellizzia, A.; Pimentel, N. *Terreno Mérida: Un Cinturón Alóctono Herciniano En La Cordillera de Los Andes de Venezuela*; European Association of Geoscientists & Engineers location: Caracas, Venezuela, 1994; pp. 277–290.
52. Aleman, A.; Ramos, V.A. The Northern Andes. In *Tectonic Evolution of South America*; SciELO Analytics: Santiago de Chile, Chile, 2000; pp. 453–480.
53. Mejia, M.I.A.; Garcia, G.Z.; Martens, U. Caracterización Petrográfica, Geoquímica y Edad de La Sienita Nefelínica de San José Del Guaviare. *Boletín Geol.* **2012**, *34*, 15–26.
54. Omarini, R.H.; Sureda, R.J.; Götze, H.-J.; Seilacher, A.; Pflüger, F. Puncoviscana Folded Belt in Northwestern Argentina: Tes-timony of Late Proterozoic Rodinia Fragmentation and Pre-Gondwana Collisional Episodes. *Int. J. Earth Sci.* **1999**, *88*, 76–97. [CrossRef]
55. Tazzo-Rangel, M.D.; Weber, B.; Frei, D.; González-Guzmán, R. Depositional Age and Provenance of High-Grade Paragneisses from the Mérida Andes, Venezuela: Implications for the Ediacaran–Cambrian Tectonic Setting of Northwestern Gondwana. *Lithos* **2021**, *404–405*, 106436. [CrossRef]
56. Chew, D.M.; Schaltegger, U.; Kosler, J.; Whitehouse, M.J.; Gutjahr, M.; Spikings, R.A.; Miskovic, A. U-Pb Geochronologic Evidence for the Evolution of the Gondwanan Margin of the North-Central Andes. *Geol. Soc. Am. Bull.* **2007**, *119*, 697–711. [CrossRef]
57. Gutiérrez, E.G.; Horton, B.K.; Vallejo, C.; Jackson, L.J.; George, S.W.M. Provenance and geochronological insights into late cretaceous-cenozoic foreland basin development in the subandean zone and oriente basin of Ecuador. In *Andean Tectonics*; Elsevier: Amsterdam, The Netherlands, 2019; pp. 237–268. ISBN 978-0-12-816009-1.
58. Bahlburg, H.; Vervoort, J.D.; Du Frane, S.A.; Bock, B.; Augustsson, C.; Reimann, C. Timing of Crust Formation and Recycling in Accretionary Orogens: Insights Learned from the Western Margin of South America. *Earth Sci. Rev.* **2009**, *97*, 215–241. [CrossRef]
59. Piraquive, A.; Kammer, A.; Gómez, C.; Bernet, M.; Muñoz-Rocha, J.A.; Quintero, C.A.; Laurent, O.; von Quadt, A.; Pe-ña-Urueña, M.L. Middle-Late Triassic Metamorphism of the Guajira Arch-Basement: Insights from Zircon U–Pb and Lu–Hf Systematics. *J. S. Am. Earth Sci.* **2021**, *110*, 103397. [CrossRef]
60. Aspden, J.A.; Bonilla, W.; Duque, P. *The El Oro Metamorphic Complex, Ecuador: Geology and Economic Mineral Deposits*; Overseas Geology and Mineral Resources; British Geological Survey: Nottingham, UK, 1995; p. 63.
61. Bayona, G.; Jiménez, G.; Silva, C.; Cardona, A.; Montes, C.; Roncancio, J.; Cordani, U. Paleomagnetic Data and K–Ar Ages from Mesozoic Units of the Santa Marta Massif: A Preliminary Interpretation for Block Rotation and Translations. *J. S. Am. Earth Sci.* **2010**, *29*, 817–831. [CrossRef]
62. Carrasco, H.F. *Geochronological, Geochemical and Isotopic Characterisation of the Mesozoic (160–110 Ma) Andean Margin within Ecuador*; University of Geneva: Geneva, Switzerland, 2021.
63. Nivia, A.; Marriner, G.F.; Kerr, A.C.; Tarney, J. The Quebradagrande Complex: A Lower Cretaceous Ensialic Marginal Basin in the Central Cordillera of the Colombian Andes. *J. S. Am. Earth Sci.* **2006**, *21*, 423–436. [CrossRef]
64. Jaramillo, J.S.; Cardona, A.; León, S.; Valencia, V.; Vinasco, C. Geochemistry and Geochronology from Cretaceous Magmatic and Sedimentary Rocks at 6°35′ N, Western Flank of the Central Cordillera (Colombian Andes): Magmatic Record of Arc Growth and Collision. *J. S. Am. Earth Sci.* **2017**, *76*, 460–481. [CrossRef]
65. Toussaint, J.F.; Restrepo, J.J. The Colombian Andes during cretaceous times. In *Cretaceous Tectonics of the Andes*; Salfity, J.A., Ed.; Vieweg+Teubner Verlag: Wiesbaden, Germany, 1994; pp. 61–100, ISBN 978-3-528-06613-0.
66. Peacock, M.A. Classification of Igneous Rock Series. *J. Geol.* **1931**, *39*, 54–67. [CrossRef]
67. Maniar, P.D.; Piccoli, P.M. Tectonic Discrimination of Granitoids. *Geol. Soc. Am. Bull.* **1989**, *101*, 635–643. [CrossRef]
68. John, T.; Scherer, E.E.; Schenk, V.; Herms, P.; Halama, R.; Garbe-Schönberg, D. Subducted Seamounts in an Eclogite-Facies Ophiolite Sequence: The Andean Raspas Complex, SW Ecuador. *Contrib. Miner. Pet.* **2010**, *159*, 265–284. [CrossRef]
69. Shervais, J.W. Ti-V Plots and the Petrogenesis of Modern and Ophiolitic Lavas. *Earth Planet. Sci. Lett.* **1982**, *59*, 101–118. [CrossRef]

70. Rodriguez, G.; Zapata, G. Comparative Analysis of the Barroso Formation and Quebradagrande Complex: A Volcanic Arc Tholeiitic-Calcoalcaline, Segmented by the Fault System Romeral in Northern Andes. *Bol. Cienc. Tierra.* **2013**, *33*, 39–58.
71. Van der Lelij, R.; Spikings, R.; Gerdes, A.; Chiaradia, M.; Vennemann, T.; Mora, A. Multi-Proxy Isotopic Tracing of Magmatic Sources and Crustal Recycling in the Palaeozoic to Early Jurassic Active Margin of North-Western Gondwana. *Gondwana Res.* **2019**, *66*, 227–245. [CrossRef]
72. Stacey, J.S.; Kramers, J.D. Approximation of Terrestrial Lead Isotope Evolution by a Two-Stage Model. *Earth Planet. Sci. Lett.* **1975**, *26*, 207–221. [CrossRef]
73. Astini, R.A.; Benedetto, J.L.; Vaccari, N.E. The Early Paleozoic Evolution of the Argentine Precordillera as a Laurentian Rifted, Drifted, and Collided Terrane: A Geodynamic Model. *Geol. Soc. Am. Bull.* **1995**, *107*, 253–0273. [CrossRef]
74. Harris, C.; Faure, K.; Diamond, R.E.; Scheepers, R. Oxygen and Hydrogen Isotope Geochemistry of S- and I-Type Granitoids: The Cape Granite Suite, South Africa. *Chem. Geol.* **1997**, *143*, 95–114. [CrossRef]
75. Ruiz, J.; Tosdal, R.M.; Restrepo, P.A.; Murillo-Muneton, G. Pb Isotope Evidence for Colombia–Southern México Connections in the Proterozoic. *Geol. Soc. Am. Spec. Pap.* **1999**, *336*, 183–197.
76. Tosdal, R.M. The Amazon-Laurentian Connection as Viewed from the Middle Proterozoic Rocks in the Central Andes, Western Bolivia and Northern Chile. *Tectonics* **1996**, *15*, 827–842. [CrossRef]
77. Gerdes, A.; Zeh, A. Combined U–Pb and Hf Isotope LA-(MC-)ICP-MS Analyses of Detrital Zircons: Comparison with SHRIMP and New Constraints for the Provenance and Age of an Armorican Metasediment in Central Germany. *Earth Planet. Sci. Lett.* **2006**, *249*, 47–61. [CrossRef]
78. Ordóñez-Carmona, O.; Álvarez, J.J.R.; Pimentel, M.M. Geochronological and Isotopical Review of Pre-Devonian Crustal Basement of the Colombian Andes. *J. S. Am. Earth Sci.* **2006**, *21*, 372–382. [CrossRef]
79. Bingen, B.; Demaiffe, D. Geochemical Signature of the Egersund Basaltic Dyke Swarm, SW Norway, in the Context of Late-Neoproterozoic Opening of the Iapetus Ocean. *Nor. Geol. Tidsskr.* **1999**, *79*, 69–86. [CrossRef]
80. Spikings, R.A.; Winkler, W.; Seward, D.; Handler, R. Along-Strike Variations in the Thermal and Tectonic Response of the Continental Ecuadorian Andes to the Collision with Heterogeneous Oceanic Crust. *Earth Planet. Sci. Lett.* **2001**, *186*, 57–73. [CrossRef]
81. Vallejo, C.; Spikings, R.A.; Luzieux, L.; Winkler, W.; Chew, D.; Page, L. The Early Interaction between the Caribbean Plateau and the NW South American Plate: Caribbean Plateau-South American Plate Collision. *Terra Nova* **2006**, *18*, 264–269. [CrossRef]
82. Spikings, R.A.; Popov, D.V. Thermochronology of Alkali Feldspar and Muscovite at T > 150 °C Using the 40Ar/39Ar Method: A Review. *Minerals* **2021**, *11*, 1025. [CrossRef]
83. Van der Lelij, R.; Spikings, R.; Mora, A. Thermochronology and Tectonics of the Mérida Andes and the Santander Massif, NW South America. *Lithos* **2016**, *248–251*, 220–239. [CrossRef]
84. Cochrane, R.; Spikings, R.A.; Chew, D.; Wotzlaw, J.-F.; Chiaradia, M.; Tyrrell, S.; Schaltegger, U.; Van der Lelij, R. High Temperature (>350 °C) Thermochronology and Mechanisms of Pb Loss in Apatite. *Geochim. Cosmochim. Acta* **2014**, *127*, 39–56. [CrossRef]
85. Spikings, R.A.; Crowhurst, P.V.; Winkler, W.; Villagomez, D. Syn- and Post-Accretionary Cooling History of the Ecuadorian Andes Constrained by Their in-Situ and Detrital Thermochronometric Record. *J. S. Am. Earth Sci.* **2010**, *30*, 121–133. [CrossRef]
86. Villagómez, D.; Spikings, R. Thermochronology and Tectonics of the Central and Western Cordilleras of Colombia: Early Cretaceous–Tertiary Evolution of the Northern Andes. *Lithos* **2013**, *160–161*, 228–249. [CrossRef]
87. Jaimes, E.; de Freitas, M. An Albian–Cenomanian Unconformity in the Northern Andes: Evidence and Tectonic Significance. *J. S. Am. Earth Sci.* **2006**, *21*, 466–492. [CrossRef]
88. Balkwill, H.R.; Paredes, F.I.; Rodriguez, G.; Almeida, J.P. Northern part of oriente basin, Ecuador: Reflection seismic expres-sion of structures. In *Petroleum Basins of South America*; American Association of Petroleum Geologists: Tulsa, OK, USA, 1995; Volume 62, pp. 559–571.
89. Jaillard, E.; Soler, P.; Carlier, G.; Mourier, T. Geodynamic Evolution of the Northern and Central Andes during Early to Middle Mesozoic Times: A Tethyan Model. *J. Geol. Soc.* **1990**, *147*, 1009–1022. [CrossRef]
90. Sarmiento, L.F.; Rangel, A. Petroleum Systems of the Upper Magdalena Valley, Colombia. *Mar. Pet. Geol.* **2004**, *21*, 373–391. [CrossRef]
91. Kennan, L.; Pindell, J.L. Dextral Shear, Terrane Accretion and Basin Formation in the Northern Andes: Best Explained by Interaction with a Pacific-Derived Caribbean Plate? *Geol. Soc. Lond. Spec. Publ.* **2009**, *328*, 487–531. [CrossRef]
92. Ruiz, G.M.H.; Seward, D.; Winkler, W. Chapter 36 Evolution of the Amazon basin in Ecuador with special reference to hinterland tectonics: Data from zircon fission-track and heavy mineral analysis. In *Developments in Sedimentology*; Elsevier: Amsterdam, The Netherlands, 2007; Volume 58, pp. 907–934. ISBN 978-0-444-51753-1.
93. Villagómez, D.; Spikings, R.; Mora, A.; Guzmán, G.; Ojeda, G.; Cortés, E.; van der Lelij, R. Vertical Tectonics at a Continental Crust-Oceanic Plateau Plate Boundary Zone: Fission Track Thermochronology of the Sierra Nevada de Santa Marta, Colombia: Thermochronology of Northern Colombia. *Tectonics* **2011**, *30*. [CrossRef]
94. Ernst, R.E.; Bell, K. Large Igneous Provinces (LIPs) and Carbonatites. *Min. Pet.* **2010**, *98*, 55–76. [CrossRef]
95. Tegner, C.; Andersen, T.B.; Kjøll, H.J.; Brown, E.L.; Hagen-Peter, G.; Corfu, F.; Planke, S.; Torsvik, T.H. A Mantle Plume Origin for the Scandinavian Dyke Complex: A "Piercing Point" for 615 Ma Plate Reconstruction of Baltica? *Geochem. Geophys. Geosyst.* **2019**, *20*, 1075–1094. [CrossRef]

96. Dalziel, I.W.D. Overview: Neoproterozoic-Paleozoic Geography and Tectonics: Review, Hypothesis, Environmental Speculation. *Geol. Soc. Am. Bull.* **1997**, *109*, 16–42. [CrossRef]
97. Nance, R.D.; Murphy, J.B. Supercontinents and the Case for Pannotia. *Geol. Soc. Lond. Spec. Publ.* **2019**, *470*, 65–86. [CrossRef]
98. Baldo, E.; Casquet, C.; Pankhurst, R.J.; Galindo, C.; Rapela, C.W.; Fanning, C.M.; Dahlquist, J.; Murra, J. Neoproterozoic A-Type Magmatism in the Western Sierras Pampeanas (Argentina): Evidence for Rodinia Break-up along a Proto-Iapetus Rift? *Terra Nova* **2006**, *18*, 388–394. [CrossRef]
99. Tollo, R.P.; Aleinikoff, J.N.; Bartholomew, M.J.; Rankin, D.W. Neoproterozoic A-Type Granitoids of the Central and Southern Appalachians: Intraplate Magmatism Associated with Episodic Rifting of the Rodinian Supercontinent. *Precambrian Res.* **2004**, *128*, 3–38. [CrossRef]
100. Cocks, L.R.M.; Torsvik, T.H. Earth Geography from 500 to 400 Million Years Ago: A Faunal and Palaeomagnetic Review. *J. Geol. Soc.* **2002**, *159*, 631–644. [CrossRef]
101. Dickinson, W.R.; Lawton, T.F. Carboniferous to Cretaceous Assembly and Fragmentation of Mexico. *Geol. Soc. Am. Bull.* **2001**, *113*, 1142–1160. [CrossRef]
102. Elías-Herrera, M.; Ortega-Gutiérrez, F. Caltepec Fault Zone: An Early Permian Dextral Transpressional Boundary between the Proterozoic Oaxacan and Paleozoic Acatlán Complexes, Southern Mexico, and Regional Tectonic Implications: Caltepec Fault Zone. *Tectonics* **2002**, *21*, 4–18. [CrossRef]
103. Restrepo-Pace, P.A.; Cediel, F. Northern South America Basement Tectonics and Implications for Paleocontinental Recon-structions of the Americas. *J. S. Am. Earth Sci.* **2010**, *29*, 764–771. [CrossRef]
104. Dalziel, I.W.D. Collision and Cordilleran Orogenesis: An Andean Perspective. *Geol. Soc. Lond. Spec. Publ.* **1986**, *19*, 389–404. [CrossRef]
105. Gutscher, M.-A. Andean Subduction Styles and Their Effect on Thermal Structure and Interplate Coupling. *J. S. Am. Earth Sci.* **2002**, *15*, 3–10. [CrossRef]
106. Collins, W.J. Hot Orogens, Tectonic Switching, and Creation of Continental Crust. *Geol. J.* **2002**, *30*, 535. [CrossRef]
107. Lucassen, F.; Franz, G. The Early Palaeozoic Orogen in the Central Andes: A Non-Collisional Orogen Comparable to the Ce-nozoic High Plateau? *Geol. Soc. Lond. Spec. Publ.* **2005**, *246*, 257–273. [CrossRef]
108. Kemp, A.I.S.; Hawkesworth, C.J.; Collins, W.J.; Gray, C.M.; Blevin, P.L. Isotopic Evidence for Rapid Continental Growth in an Extensional Accretionary Orogen: The Tasmanides, Eastern Australia. *Earth Planet. Sci. Lett.* **2009**, *284*, 455–466. [CrossRef]
109. Murphy, J.B.; Fernandez-Suarez, J.; Jeffries, T.; Strachan, R. U–Pb (LA–ICP-MS) Dating of Detrital Zircons from Cambrian Clastic Rocks in Avalonia: Erosion of a Neoproterozoic Arc along the Northern Gondwanan Margin. *J. Geol. Soc.* **2004**, *161*, 243–254. [CrossRef]
110. Linnemann, U.; Pereira, F.; Jeffries, T.E.; Drost, K.; Gerdes, A. The Cadomian Orogeny and the Opening of the Rheic Ocean: The Diachrony of Geotectonic Processes Constrained by LA-ICP-MS U–Pb Zircon Dating (Ossa-Morena and Saxo-Thuringian Zones, Iberian and Bohemian Massifs). *Tectonophysics* **2008**, *461*, 21–43. [CrossRef]
111. Nance, R.D.; Gutiérrez-Alonso, G.; Keppie, J.D.; Linnemann, U.; Murphy, J.B.; Quesada, C.; Strachan, R.A.; Woodcock, N.H. Evolution of the Rheic Ocean. *Gondwana Res.* **2010**, *17*, 194–222. [CrossRef]
112. Van Staal, C.R.; Barr, S.M.; Murphy, J.B. Provenance and Tectonic Evolution of Ganderia: Constraints on the Evolution of the Iapetus and Rheic Oceans. *Geology* **2012**, *40*, 987–990. [CrossRef]
113. Solari, L.A.; Ortega-Gutiérrez, F.; Elías-Herrera, M.; Gómez-Tuena, A.; Schaaf, P. Refining the Age of Magmatism in the Altos Cuchumatanes, Western Guatemala, by LA–ICPMS, and Tectonic Implications. *Int. Geol. Rev.* **2010**, *52*, 977–998. [CrossRef]
114. Keppie, J.D.; Dostal, J.; Miller, B.V.; Ramos-Arias, M.A.; Morales-Gámez, M.; Nance, R.D.; Murphy, J.B.; Ortega-Rivera, A.; Lee, J.W.K.; Housh, T.; et al. Ordovician–Earliest Silurian Rift Tholeiites in the Acatlán Complex, Southern Mexico: Evidence of Rifting on the Southern Margin of the Rheic Ocean. *Tectonophysics* **2008**, *461*, 130–156. [CrossRef]
115. Spikings, R.; Reitsma, M.J.; Boekhout, F.; Mišković, A.; Ulianov, A.; Chiaradia, M.; Gerdes, A.; Schaltegger, U. Characterisation of Triassic Rifting in Peru and Implications for the Early Disassembly of Western Pangaea. *Gondwana Res.* **2016**, *35*, 124–143. [CrossRef]
116. Kirsch, M.; Keppie, J.D.; Murphy, J.B.; Solari, L.A. Permian-Carboniferous Arc Magmatism and Basin Evolution along the Western Margin of Pangea: Geochemical and Geochronological Evidence from the Eastern Acatlan Complex, Southern Mexico. *Geol. Soc. Am. Bull.* **2012**, *124*, 1607–1628. [CrossRef]
117. Solari, L.A.; Ortega-Gutiérrez, F.; Elías-Herrera, M.; Schaaf, P.; Norman, M.; de León, R.T.; Ortega-Obregón, C.; Chiquín, M.; Ical, S.M. U-Pb Zircon Geochronology of Palaeozoic Units in Western and Central Guatemala: Insights into the Tectonic Evolution of Middle America. *Geol. Soc. Lond. Spec. Publ.* **2009**, *328*, 295–313. [CrossRef]
118. Stewart, J.H.; Blodgett, R.B.; Boucot, A.J.; Carter, J.L.; Lopez, R. Exotic paleozoic strata of Gondwanan provenance near ciudad Victoria, Tamaulipas, Mexico. In *Laurentia-Gondwana Connections Before Pangaea*; Geological Society of America: Boulder, CO, USA, 1999; Volume 336, pp. 227–252.
119. Lopez, R. *High-Mg Andesites from the Gila Bend Mountains: Evidence for Hydrous Melting of the Lithosphere during Miocene Ex-Tension, and the Pre-Jurassic Geotectonic Evolution of the Coahuila Terrane, Northeastern Mexico: Grenville Basement, a Late Paleozoic Arc, Triassic Plutonism, and the Events South of the Ouachita Suture*; University of California Santa Cruz: Santa Cruz, CA, USA, 1997.
120. Pindell, J.; Dewey, J.F. Permo-Triassic Reconstruction of Western Pangea and the Evolution of the Gulf of Mexico and South Caribbean Region. *Tectonics* **1982**, *1*, 179–211. [CrossRef]

121. Macdonald, W.D.; Hurley, P.M. Precambrian Gneisses from Northern Colombia, South America. *Geol. Soc. Am. Bull.* **1969**, *80*, 1867. [CrossRef]
122. Collins, W.J.; Richards, S.W. Geodynamic Significance of S-Type Granites in Circum-Pacific Orogens. *Geology* **2008**, *36*, 559. [CrossRef]
123. Senff, M. *Sedimentologie, Fauna Und Fazies des Präkretazischen Mesozoikum Im Oberen Magdalenatal von Zentralkolumbien Unter Besonderer Berüecksichtigung der Obertriassischen Payande Formation*; Univeristät Giessen: Giessen, Germany, 1995.
124. Cediel, F.; Caceres, C. *Geological Map of Colombia*; Geotec, Ltd.: Bogotá, Colombia, 2000.
125. Kay, S.M.; Burns, W.M.; Copeland, P.; Mancilla, O. Upper cretaceous to holocene magmatism and evidence for transient miocene shallowing of the Andean subduction zone under the Northern Neuquén basin. In *Evolution of an Andean Margin: A Tectonic and Magmatic View from the Andes to the Nequen Basin (35°–39° S Lat)*; Geological Society of America: Boulder, CO, USA, 2006; Volume 407, pp. 19–59.
126. Pratt, W.T.; Duque, P.; Ponce, M. An Autochthonous Geological Model for the Eastern Andes of Ecuador. *Tectonophysics* **2005**, *399*, 251–278. [CrossRef]
127. Mora, A.; Parra, M.; Strecker, M.R.; Sobel, E.R.; Hooghiemstra, H.; Torres, V.; Jaramillo, J.V. Climatic Forcing of Asymmetric Orogenic Evolution in the Eastern Cordillera of Colombia. *Geol. Soc. Am. Bull.* **2008**, *120*, 930–949. [CrossRef]
128. Mora, A.; Gaona, T.; Kley, J.; Montoya, D.; Parra, M.; Quiroz, L.I.; Reyes, G.; Strecker, M.R. The Role of Inherited Extensional Fault Segmentation and Linkage in Contractional Orogenesis: A Reconstruction of Lower Cretaceous Inverted Rift Basins in the Eastern Cordillera of Colombia. *Basin Res.* **2009**, *21*, 111–137. [CrossRef]
129. Tesón, E.; Mora, A.; Silva, A.; Namson, J.; Teixell, A.; Castellanos, J.; Casallas, W.; Julivert, M.; Taylor, M.; Ibáñez-Mejía, M.; et al. Relationship of Mesozoic Graben Development, Stress, Shortening Magnitude, and Structural Style in the Eastern Cordillera of the Colombian Andes. *Geol. Soc. Lond. Spec. Publ.* **2013**, *377*, 257–283. [CrossRef]